Cy 2

AD A035 692

AMMRC CTR 76-40

NOISE ABATEMENT AND INTERNAL VIBRATIONAL ABSORPTION IN POTENTIAL STRUCTURAL MATERIALS

November 1976

L. Kaufman, S. A. Kulin, P. P. Neshe

ManLabs, Inc.
21 Erie Street
Cambridge, Massachusetts 02139

Interim Report   Contract Number DAAG46-74-C-0048

Sponsored by: Defense Advanced Research Projects Agency
ARPA Order No. 2555

Program Code No. 7 D 10
Effective Date of Contract: 30 November 1973
Contract Expiration Date: 30 December 1976
Amount of Contract: $635,454.00
Contract Period Covered by Report: 1 March 1976 to 1 September 1976

Approved for public release; distribution unlimited.

Prepared for

ARMY MATERIALS AND MECHANICS RESEARCH CENTER
Watertown, Massachusetts 02172

UNCLASSIFIED

SECURITY CLASSIFICATION OF THIS PAGE (When Data Entered)

REPORT DOCUMENTATION PAGE

READ INSTRUCTIONS BEFORE COMPLETING FORM

1. REPORT NUMBER AMMRC CTR	2. GOVT ACCESSION NO.	3. RECIPIENT'S CATALOG NUMBER
4. TITLE (and Subtitle)		5. TYPE OF REPORT & PERIOD COVERED Semi-annual Report No. 5 1 March 1976 - 1 Sept. 1976
		6. PERFORMING ORG. REPORT NUMBER
7. AUTHOR(s)		8. CONTRACT OR GRANT NUMBER(s) DAAG46-74-C-0048
9. PERFORMING ORGANIZATION NAME AND ADDRESS		10. PROGRAM ELEMENT, PROJECT, TASK AREA & WORK UNIT NUMBERS ARPA Order No: 2555 Program Code No: 7 DIO
11. CONTROLLING OFFICE NAME AND ADDRESS Army Materials and Mechanics Research Center Watertown, Massachusetts 02172		12. REPORT DATE November 1976
		13. NUMBER OF PAGES
14. MONITORING AGENCY NAME & ADDRESS(if different from Controlling Office)		15. SECURITY CLASS. (of this report) Unclassified
		15a. DECLASSIFICATION/DOWNGRADING SCHEDULE

16. DISTRIBUTION STATEMENT (of this Report)

Approved for public release; distribution unlimited.

17. DISTRIBUTION STATEMENT (of the abstract entered in Block 20, if different from Report)

18. SUPPLEMENTARY NOTES

19. KEY WORDS (Continue on reverse side if necessary and identify by block number)

Vibration Damping	Internal Friction
Sound Transmission	Iron-Cobalt Alloys
Titanium - Nickel Alloy	Copper-Aluminum-Nickel Alloys

20. ABSTRACT (Continue on reverse side if necessary and identify by block number)

Efforts have been directed toward identifying potential structural materials which can combine high strength and damping characteristic in the audible range. Cobalt-iron alloys with additions of aluminum and manganese, copper-aluminum-nickel alloys, iron-chromium-aluminum alloys, titanium-nickel alloys, and several commerical steel compositions have been investigated. The range of yield strengths and loss factors which are attainable exceed currently available commercial materials.

DD FORM 1 JAN 73 1473 EDITION OF 1 NOV 65 IS OBSOLETE

UNCLASSIFIED

SECURITY CLASSIFICATION OF THIS PAGE (When Data Entered)

Measurements of the enthalpy of transformation in a thermoelastic Cu-Al-Ni alloy has been conducted over a range of grain size and sample size to assess the stored elastic strain energy. Studies of the magnetic domain wall configuration in a cobalt-iron alloy have been carried out to evaluate the contribution of domains to damping in this alloy.

The hull of a one-sixth scale dynamic model of an armoured personnel carrier is being fabricated from a high damping iron-chromium-aluminum for evaluation over a range of vibrational frequencies simulating operation. A torpedo propeller has been cast from a high damping cobalt-iron alloy for evaluation in a simulated vibration test.

FOREWORD

This research was supported by the Advanced Research Projects Agency of the Department of Defense and was monitored by the Army Materials and Mechanics Research Center under Contract No. DAAF46-74-C-0048. The research studies reported here were conducted by personnel at ManLabs, Inc. with the collaboration of Professor Morris Cohen, Professor Walter S. Owen, and Dr. Richard Salzbrenner of the Department of Materials Science, Massachusetts Institute of Technology, Dr. J. Heine of Bolt, Beranek and Newman, and Dr. Richard J. Weiss of Army Mechanics and Materials Research Center.

TABLE OF CONTENTS

LIST OF TABLES

LIST OF FIGURES

LIST OF FIGURES (continued)

LIST OF FIGURES (continued)

I. INTRODUCTION AND SUMMARY

The utilization of structural materials capable of suppressing noise and vibration offers substantial advantages in the design of a wide range of military applications. In particular ship and helicopter propulsion, tracked land vehicle and torpedo propulsion systems would all operate more efficiently if materials capable of absorbing noise and vibration were available for incorporation into the structure.

The present study is aimed at identifying potential structural materials which exhibit high damping capacity (or loss factors) at frequencies in the audible range (i.e. 20-4000 cycles per second) and evaluating the mechanism by which damping takes place. In addition characterization of the mechanical properties such as yield strength and Youngs modulus has also been carried out to evaluate the potential use of the material as a structural element. Finally cost and fabrication factors have also been considered in order to gain some insight into the practical application of these materials in specific military systems.

Novel damping materials such as Nitinol (Ni-Ti) and copper-aluminum-nickel alloys which appear to derive their damping characteristics from thermoelastic martensitic transformations have been investigated. The results have been documented in previous reports (1,3).* In addition, commercial damping materials such as Nivco (Co-Ni-Ti-Al) and Incramute (Cu-Mn-Al) have also been evaluated in order to develop a basis for comparison. In the course of the present study (2) a family of cobalt-iron alloys which can be carefully heat treated to yield very high damping characteristics has been synthesized. Although the mechanism leading to the high loss factors which characterize these alloys is not clear, it appears that the structure which provides the desirable high loss factor is a metastable fcc solid solution. The

*Underscored numbers in parentheses denote references.

80 w/o Co-20 w/o Fe alloy, which is the base for this family, is readily cast, forged and cold worked, has been fabricated into rod by swaging and cold rolled into 50 mil foil indicating that it could be employed in a variety of applications.

Figure 1 shows a bar graph comparing the loss factors of a number of materials under investigation at present in our study. The 0.2 percent offset yield strength is also shown for each material (please note that the loss factor is shown on logarithmic scale). The commercial materials Nivco and Incramute are in the condition supplied by commercial vendors. The results for Nitinol displayed in Figure 1 have been optimized (2) through a 15% reduction in thickness by rolling at room temperature. The bar graphs for Co-Fe, Co-Fe-Al and Co-Fe-Mn represent data taken on annealed samples of the experimental alloys currently under study which have been synthesized in the present program. All of the data displayed in Figure 1 refer to 25°C. The loss factors reported were determined by the resonant dwell method (1,2) using a cantilevered beam at a peak stress of 2000 psi. It is well known that many materials show increased loss factors at higher stress (4-8). Indeed such performance may be of critical importance in actual design. Similarly loss factors (Q^{-1}) are known to vary substantially with frequency and usually increase as the frequency is decreased from the audible range to the 1 cycle/sec range. However present consideration has been restricted to frequencies near 200 Hertz (cycles/sec) at low stress levels.

Figure 1 shows that the Co-Fe alloy can develop loss factors near 0.04 (i.e. 4 percent). However the yield strength is low, 18000 psi. The closest competitor is Incramute which exhibits a loss factor of 2 percent. However Incramute has a higher yield strength, 45000 psi. The remaining commercial material, Nivco, has a low damping capacity near 0.1 percent but a high yield strength of 108,000 psi.

In the past two years efforts have been directed

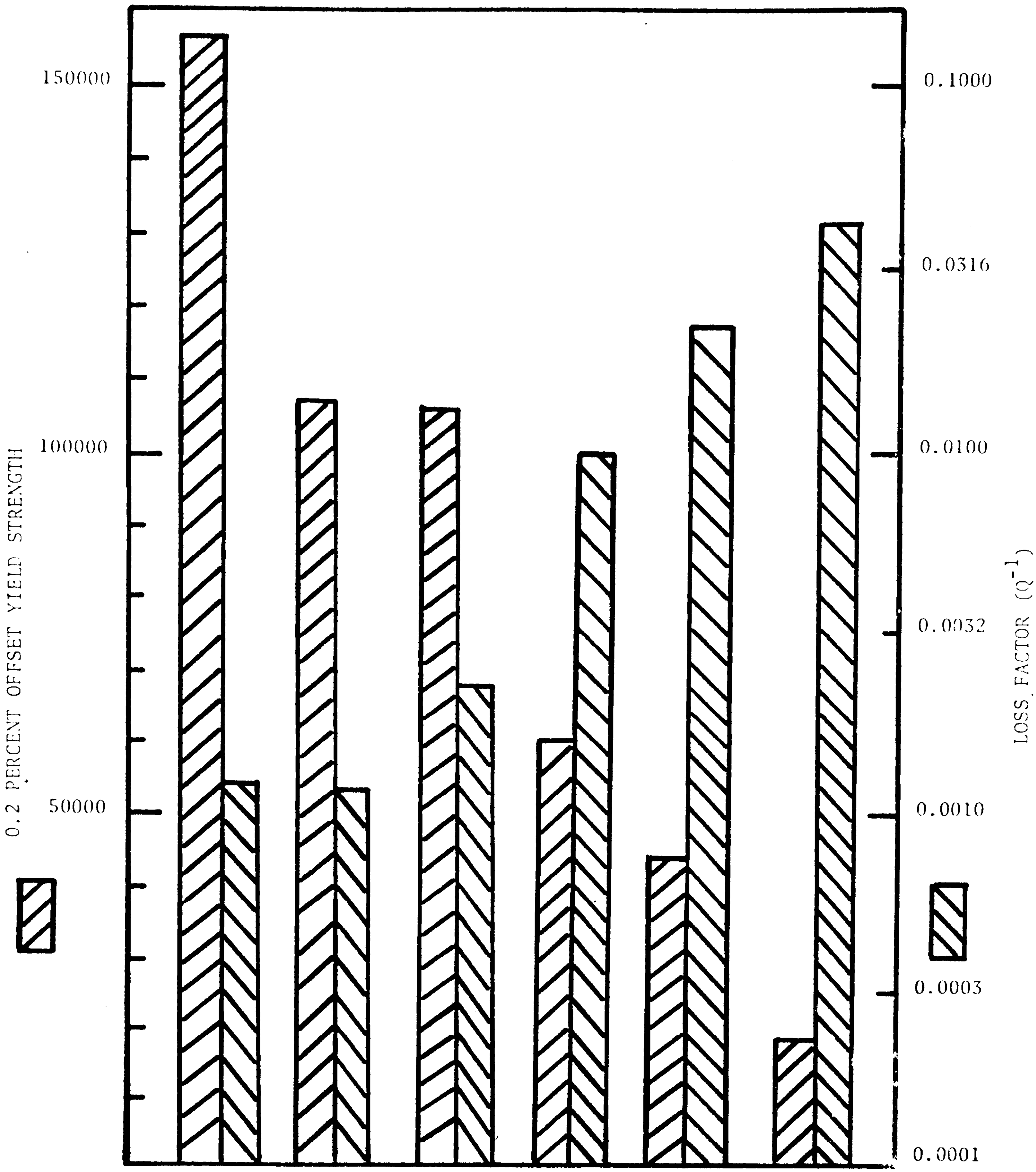

Figure 1. Comparison of Loss Factors and Yield Strength at 25°C for Several Materials. Loss Factor is measured at 2000 psi peak stress and 150-250 Hertz.

towards achieving higher yield strengths in the Co-Fe alloy by additions of nickel, aluminum and manganese. The bar graph in Figure 1 shows results obtained with small additions of aluminum and manganese. In the former case very high yield strengths in excess of 150,000 psi were attained. However this alloy exhibited a loss factor of only 0.1 percent (i.e., like Nivco). Addition of manganese resulted in yield strengths over 100,000 psi coupled with loss factors near 0.3 percent. Thus it appears that a range of loss factors and yield strengths are attainable via alloying the Co-Fe base composition. Current efforts are directed toward optimization of these properties.

An additional facet of the damping factor/mechanical property characteristics of these materials is shown in Figure 2 where the temperature dependence of the loss factor is shown for Nitinol, Incramute and the cobalt-iron alloys. These results indicate that the cobalt-iron alloy maintains high damping characteristics up to 100°C. By contrast Incramute and Nitinol display loss factors below 0.4 percent (i.e, one-tenth that of Co-Fe) above 80°C. Clearly the cobalt-iron alloy offers considerable advantages as a damping material.

During the past year additional studies of ternary additions to the base 80 w/o cobalt-20 w/o iron composition have been carried out. In particular the effects on aluminum and manganese have been explored. In the case of the former, it was found that very substantial increases in the yield strength (i.e.,from 20,000 psi to 145,000 psi) can be attained on annealed samples of the 80 Co- 20 Fe alloy when the aluminum content increases from 0 w/o to 2.5 w/o. Unfortunately this seven fold increase in strength (which is characterized by a hardness increase from RB 30 to RC 44) is accompanied by a decrease in the loss factor from four percent to 0.2 percent. Although this combination of properties is not attractive for a structural damping material, the hardening effect of aluminum in the cobalt-iron alloys could be employed as the basis for case hardening the

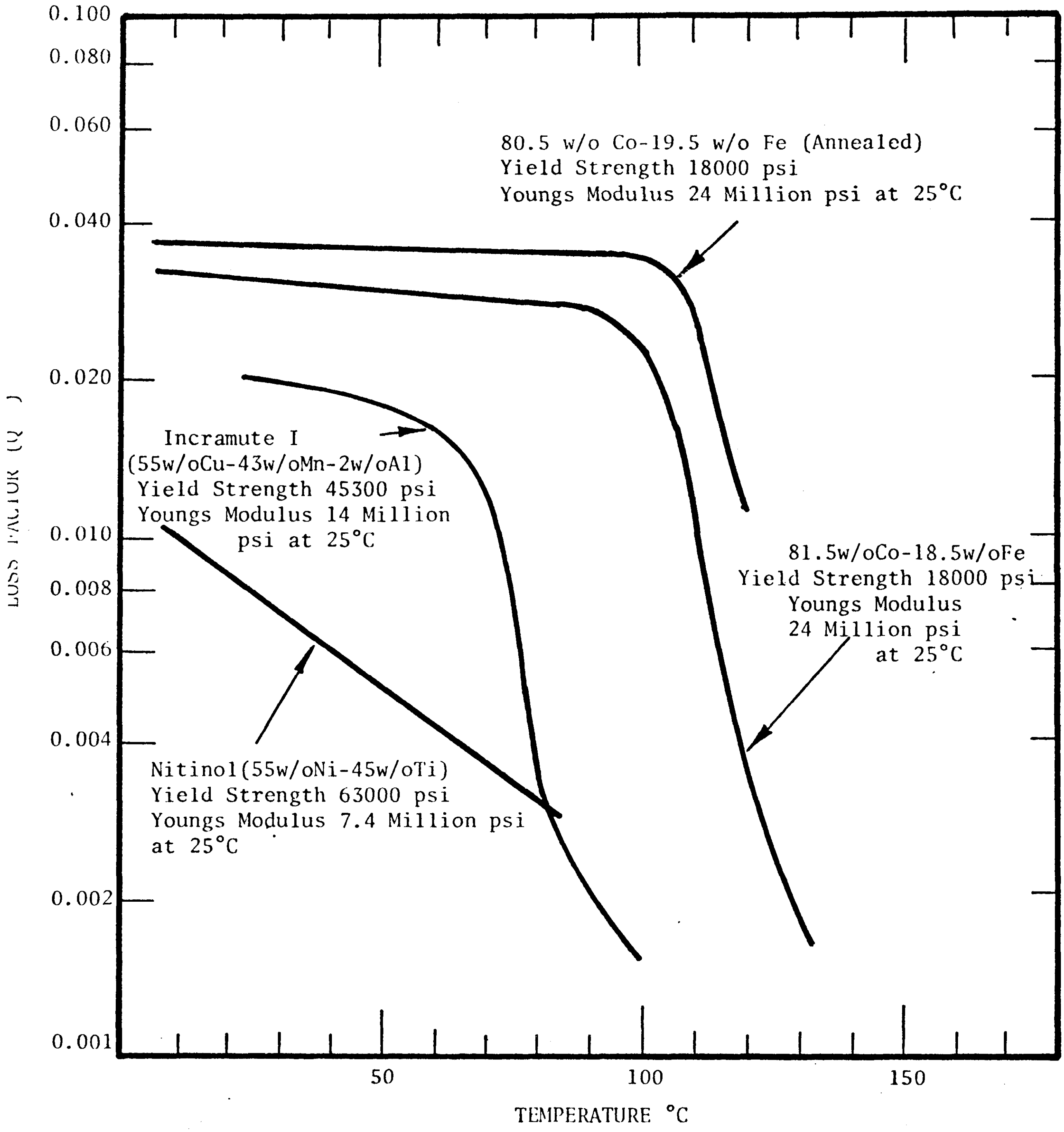

Figure 2. Comparison of the Loss Factor-Temperature Curves for Nitinol, Incramute I and Cobalt-Iron Alloys measured at a stress of 2000 psi in the Frequency Range from 150 to 250 Hertz.

latter where combinations of damping and wear resistance are desired. Manganese additions to the 80 Co-20 Fe base composition were also found to increase the strength and decrease the loss factor. However, current studies of a series of Co-Fe-Mn alloys suggest that a trade-off in properties may be realized with addition of approximately 4 w/o manganese.

Investigation of iron-chromium base alloys (85 w/o Fe-15 w/o Cr-3 w/o Aℓ and 86 w/o Fe-14 w/o Cr-0.05 w/oC) simulating a commercial Japanese damping alloy and type 405 stainless steel has disclosed additional potential damping materials with yield strengths in the 37,000 - 42,000 psi range with good corrosion resistance and yield strengths between 1.5 and 3.5 percent. These materials do not show any decrease in loss factor between - 60°C and 100°C and are relatively inexpensive (i.e., $0.50 to $0.80 per pound). Measurement of the loss factor of the cobalt-iron alloy and the iron-chromium base alloys in a saturating magnetic field lead to a decrease of 15% in the loss factor of the iron-cobalt alloy and a decrease of 30% in the iron-chromium base alloys. Measurement of the loss factor of the 80 w/o Co-20 Fe alloys at 500 psi and 2000 psi yield value of 2% and 4% respectively in keeping with the generally observed relation that the loss factor is proportional to the square root of the stress.

A survey of potential applications of high damping alloys to problems of noise and vibration control was conducted to identify problems areas which could benefit from advances in damping materials technology. Three potential areas appear to merit particular consideration. These include body panels of military reconnaissence vehicles, engine oil pans, valve covers, and ship propellers. In each case ancillary properties such as corrosion and/or fatigue resistance must also be maintained in candidate materials if system improvement is to be effected.

One method of evaluating the potential advantages of a candidate high damping structural material is to fabricate a hull

of this material for the 1/6 scale dynamic model of an armoured personnel carrier constructed by Bolt Beranek and Newman under contract DAAE07-74-C-0002. A set of six 13" x 24" x 1/4" plates, one 16" x 17" x 1/4" plate and two 14" x 24" x 1/10" plates are required to provide sufficient material for fabrication of the model. A 350 lb. cobalt-iron alloy casting was obtained from Special Metals Division of Allegheny Ludlum Corporation in order to provide sufficient stock for reduction to plate via hot rolling. Unfortunately severe difficulties which were encountered due to porosity in the casting prevented fabrication of sufficient plate. Instead a full complement of plates made from the high damping iron-chromium-aluminum alloy were obtained from Toshiba Electric Company. The plates have been delivered and are currently being assembled for testing. The high damping cobalt-iron alloy is being used to cast a torpedo propeller which will be tested shortly.

Measurements of enthalpy of transformation in a thermoelastic Cu-Aℓ-Ni alloy have been taken over a range of grain sizes, and as a function of sample size, in order to assess the stored elastic strain energy contribution on multiple interface transformations. The ability of a thermoelastic martensite to "store" elastic energy is ultimately connected with its capacity to absorb or damp out vibrational energy. If the damping mechanisms are non repeatable, then the damping capacity will deteriorate with the amount of energy absorbed. However, if the energy absorbing mechanism is repeatable and the material can return to its original state then the damping capacity will not deteriorate. Thermodynamic and microstructural studies of the cobalt-iron and copper-aluminum-nickel alloys have been carried out to provide some insight into the mechanism of energy absorbtion.

II. INVESTIGATION OF COBALT-IRON ALLOYS FOR APPLICATION AS HIGH DAMPING STRUCTURAL MATERIALS

Current efforts which have been directed toward exploiting the properties of cobalt-iron alloys for the purposes of achieving high damping properties coincident with high strength (2) stem from the work of Cochardt (4) who reported on loss factors of 70 w/o Co-30 w/o Ni and Co-Fe alloys at room temperature as disclosed by torsional pendulum measurements at a frequency of one cycle/sec (i.e. one Hertz). Cochardt reported a logarithmic decrement at 25°C and a stress of 2000 psi for a 65 w/o Co-35 w/o Ni alloy of 0.18. The logarithmic decrement is the product of π times Q^{-1}. Thus

$$\zeta = \pi Q^{-1} \tag{1}$$

and if $\zeta=0.18$ then $Q^{-1} \approx 0.06$. This value is approximately fifteen times larger than the value measured in our studies (2). However, the latter values were observed at 200 Hertz (200 cycles/sec) and 2000 psi rather than 1 cycle/sec and 2000 psi stress (2). Cochardt also reported on a 80 w/o Co-20 w/o Fe alloy which exhibited $\zeta=0.09$ (i.e. $Q^{-1}=0.03$) at 1 cycle/sec and 2000 psi and 25°C. This alloy also exhibits a high Curie temperature. However, in the condition as fabricated by Cochardt (4) this alloy was a stable bcc structure which was probably ordered with no chance for transformation. The processing sequence followed by Cochardt called for homogenization at 1100°C for two hours. Figure 3 shows that the alloy was in the fcc field at this temperature (1373°K). Subsequently the alloy was annealed for two hours at 900°C (1173°K). Figure 3 shows that at this temperature the alloy was still in the stable fcc field but just about to enter the two phase fcc+bcc field. The final step in the processing sequence employed by Cochardt was a slow cool to room temperature at the rate of 120°C/hour. During this treatment the sample enters the region where the bcc

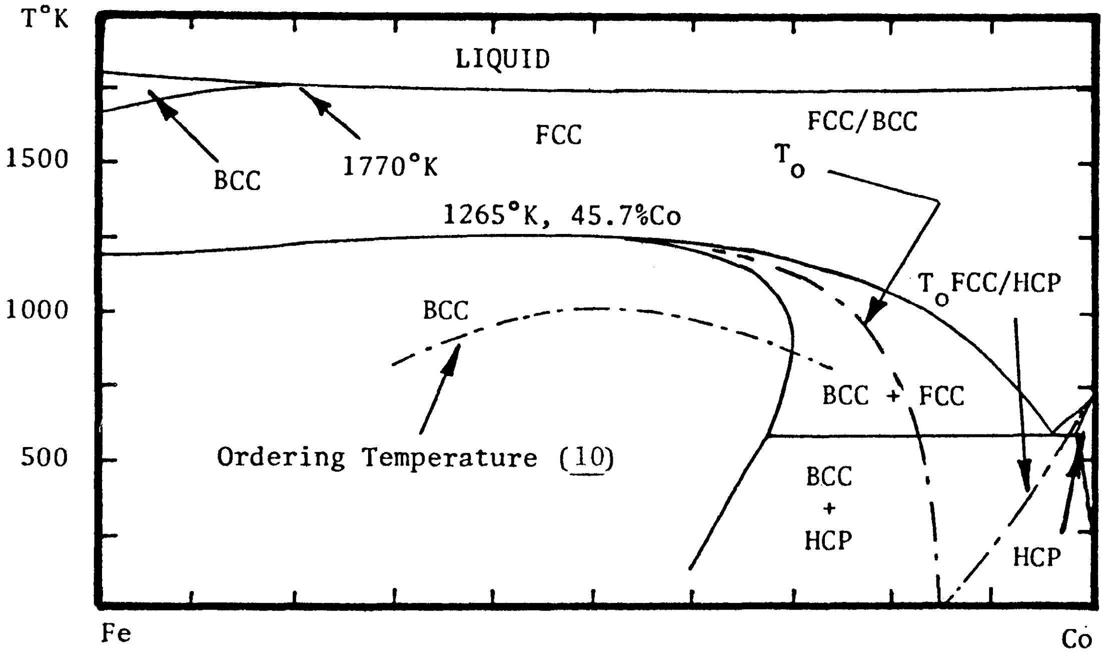

Figure 3. Calculated Iron-Cobalt Phase Diagram Showing Locus of Curve for T_o(FCC/BCC) where FCC and BCC Phases of Same Composition Have Equal Free Energies (9,10).

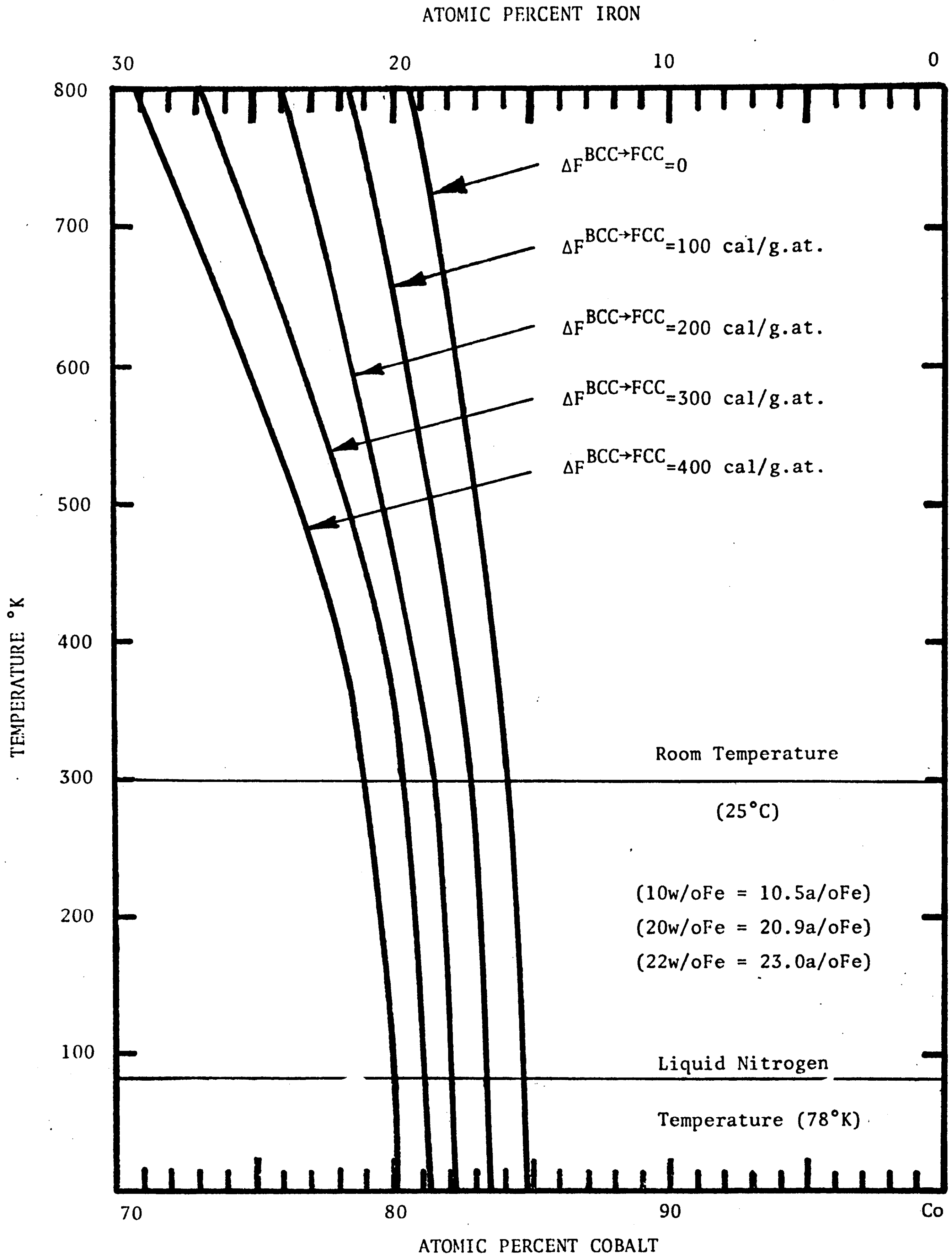

Figure 4. Calculated Temperature and Composition of the Free Energy Difference between FCC and BCC Iron Cobalt Alloys.

phase is stable and coexists with a fcc phase enriched in cobalt. In addition, the bcc orders below 800°K as is seen in Figure 3. Unfortunately Cochardt did not discuss the structure of his 80Co-20Fe alloy. However, based on his heat treatment schedule, it is likely that his alloy was largely bcc.

Figure 3 shows a curve labeled $T_o^{FCC/BCC}$ which describes the locus of points along which the fcc and bcc Co-Fe alloys have equal free energies. This curve has been computed using a thermochemical description of the fcc and bcc phases derived earlier. Figure 4 shows the free energy difference between the fcc and disordered bcc phases as a function of temperature and composition. The curve labeled $\Delta F^{BCC \rightarrow FCC} = 0$ is the same as that shown in Figure 3. The remaining curves show the locus of points corresponding to various free energy differences between disordered fcc and bcc phases. As the free energy difference becomes larger, the bcc becomes more stable relative to the fcc phase for a given composition. In the case of iron base alloys (i.e. Fe-Ni and Fe-C alloys), the fcc phase can be retained by rapid cooling until the "driving force" for transformation to the bcc form reaches the vicinity of 300 cal/g.at. (i.e. the free energy of the bcc phase is 300 cal/g.at. less than the fcc phase). Figure 4 suggests that this situation should prevail at room temperature in an alloy with 80 a/o Co-20 a/o Fe (80.9 w/o Co-19.1 w/o Fe). Alloys containing less than 20 a/o Fe could be expected to remain fcc while alloys with greater than 20 a/o (19.1 w/o) Fe would be expected to transform to the bcc phase on cooling from 1000°C. In order to test this prediction, a series of cobalt-iron alloys was prepared and air cooled from 1000°C. Figures 5-8 show the resulting microstructures. The first two photomicrographs show typical austenitic fcc structures obtained by air cooling the 82 w/o Co-18 w/o Fe and 90 w/o Co-10 w/o Fe alloys. On the other hand, Figure 7 shows the martensitic bcc structure obtained on air cooling the 78 w/o Co-22 w/o Fe alloy. The crystal structure

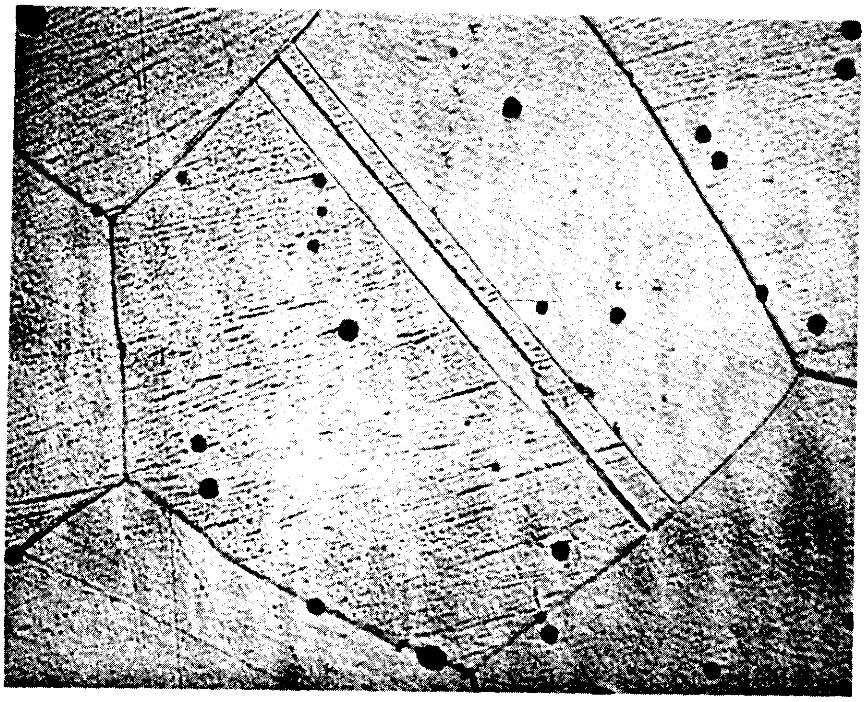

Plate No.
10486

Figure 5. 82 w/o Co-18 w/o Fe Alloy Annealed at 1000°C Air Cooled to 25°C. Etched in 5% Nital. Photomicrograph Shows Twinned Austenitic Structure (X1000).

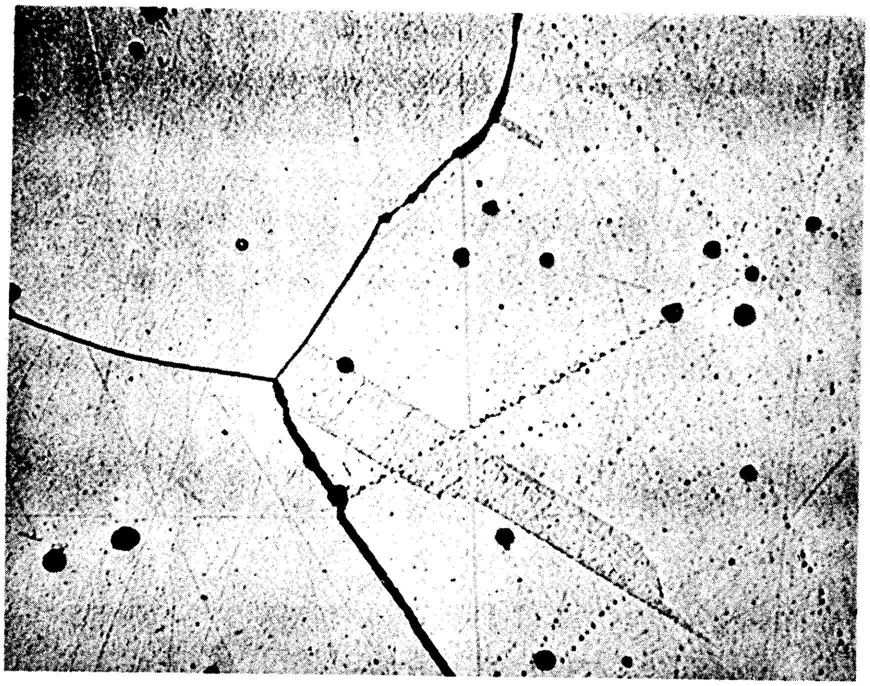

Plate No.
10489

Figure 6. 90 w/o Co-10 w/o Fe Alloy Annealed at 1000°C Air Cooled to 25°C. Etched in 5% Nital. Photomicrograph Shows Twinned Austenitic Structure (X1000).

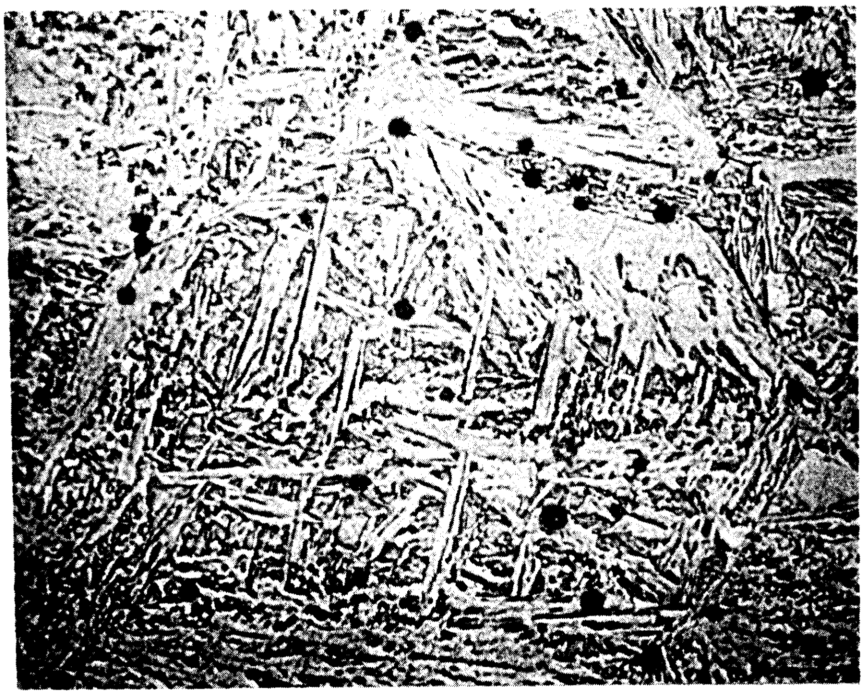

Plate No.
10483

Figure 7. 78 w/o Co-22 w/o Fe Alloy Annealed at 1000°C Air Cooled to 25°C. Etched in 5% Nital. Photomicrograph Shows Structure of BCC Phase (X1000).

Plate No.
10484

Figure 8. 80 w/o Co-20 w/o Fe Alloy Annealed at 1000°C Air Cooled to 25°C. Etched in 5% Nital. Central Grain Shows Surface Martensite (BCC) Formed during Polishing in an Austenite (FCC) Matrix (X1000).

of these alloys was verified by x-ray diffraction using CrKα radiation. Inclusions shown in Figures 5-8 are oxide particles which are present in the Ferrovac E iron used to make the alloy by combination with electrolytic cobalt.

Figure 8 shows the microstructure of the 80 w/o Co-20 w/o Fe alloy which contained some surface martensite formed during the polishing. This was established by annealing the specimen at 1000°C, air cooling it and taking an x-ray pattern from the surface without polishing. This pattern showed no bcc diffraction lines. However, polishing the surface produced strong bcc peaks. This result suggests that the 20 w/o Fe alloy (19.1 a/o Fe) is close to transforming at room temperature. This result is in keeping with the predictions of Figure 4.

An attempt was made to produce martensite in this alloy by cooling it in liquid nitrogen (i.e. to 77°K). However, no bcc phase formed. This may be due to the steep free energy difference versus temperature curve which does not yield very many more cal/g.at. of driving force as the temperature is lowered from 300°K to 77°K.

The results shown in Figures 5-8 are in keeping with earlier studies of the Co-Fe system (<u>11</u>-<u>13</u>) which showed a lowering of the fcc/hcp transition temperature of cobalt by the addition of iron. Addition of 5 a/o Fe to cobalt reduced T_o from 735°K to 500°K (<u>12</u>,<u>13</u>). Alloys with 7.5, 10.0, 12.5 and 15 a/o Fe cooled to 25°C (248°K) by water quenching after two hours at 1100°C were found to be completely fcc (<u>11</u>). Plastic deformation in Liquid nitrogen by hammering to effect a 17% deformation produced hexagonal phase in the 7.5 a/o Fe alloy and some bcc phase in the 15 a/o alloy. However the 10.0 and 12.5 a/o Fe alloys were found to remain fcc.

Thus, the series of Co-Fe alloys shown in Figures 5 and 8 with 18 and 20 w/o iron fall in exactly the range required to test the hypothesis, i.e. that high damping could be attained in

a metastable phase with a high magnetic Curie point. The Curie point for the fcc appears to be near 950°C (1223°K)(13).

Accordingly, a series of "resonant dwell damping" bars were fabricated from alloys in this series and tested at 25°C along with an additional set of alloys at a stress level near 2000 psi. The geometry of the samples resulted in natural frequencies in the 190-270 Hertz range. The results for the original set of samples are shown in Table 1 (2). This group of samples labeled 51-64 were prepared by annealing alloy stock, machining the damping bars and then making the measurements.

Subsequently, the damping bars were x-rayed. It was found that samples 57, 58, 59 and 60 (i.e. 80 w/o Co-20 w/o Fe and 82 w/o Co-18 w/o Fe) exhibited fcc and bcc diffraction lines. This was apparently due to the surface deformation which occurred during machining. Consequently, these four samples were reannealed at 1000°C and oil quenched. These samples yielded completely fcc x-ray patterns. Subsequent measurement of the loss factor yielded values of 280 to 500 x 10^{-4} as shown by samples 57A, 58A, 59A and 60A in Table 1. Following this experience, the remainder of samples 51-64 were reannealed and oil quenched and the loss factor at 25°C measured once again. The results are shown in Table 2. The reannealing did not affect the loss factors of the 78 w/o Co-22 w/o Fe samples very much. These were 14 and 16 x 10^{-4} (Numbers 55 and 56) before the reannealing and 20 and 13 x 10^{-4} (Numbers 55A and 56A) after reannealing. The diffraction patterns both showed substantial quantities of the bcc phase. Similarly, the reannealing had little effect on the 90 w/o Co-10 w/o Fe alloys. The samples 61 and 62 exhibited $Q^{-1}=8$ and 14 x 10^{-4} before reannealing and 7 and 7 x 10^{-4} after annealing. Both sets of x-ray patterns showed completely fcc structures. Thus the results show a marked peak in the loss factor in the vicinity of 80 w/o Co-20 w/o Fe providing the alloy is all fcc. This is not dependent on the magnetic Curie temperature since both the fcc and bcc phases have high Curie temperatures which

TABLE 1

SUMMARY OF RESONANT DWELL DAMPING MEASUREMENTS AT 25°C

Sample No. Composition (weight percent)	Resonant Frequency (Hz.)	Dynamical Youngs Modulus ($PSI \times 10^{-6}$)	Peak Stress (PSI)	Loss Factor ($Q^{-1} \times 10^{4}$)	Comments on Test
51(70Co-30Ni)	265	28.0	2190	66	All Samples
52(47.2Fe-52.8Pt)	185	15.7	1290	28	Annealed at
53(47.2Fe-52.8Pt)	214	19.2	1660	25	1000°C--Air
54(46.2Fe-53.8Pt)	191	14.7	1290	69	Cooled--Then
55(78.0Co-22.0Fe)	259	26.6	2050	14	Machined
56(78.0Co-22.0Fe)	251	26.3	1980	16	"
57(80.0Co-20.0Fe)	237	24.2	1790	92	"
58(80.0Co-20.0Fe)	251	24.3	1900	68	"
59(82.0Co-18.0Fe)	245	23.1	1800	81	"
60(82.0Co-18.0Fe)	237	22.8	1740	64	"
61(90.0Co-10.0Fe)	264	27.8	2140	8	"
62(90.0Co-10.0Fe)	264	28.1	2140	14	"
63(65Co-28Fe-7Ni)	240	23.2	1770	17	"
64(70Fe-20Co-10Cr)	276	29.9	2410	6	"
57A(80.0Co-20.0Fe)	238	24.4	1810	280	All Samples
58A(80.0Co-20.0Fe)	243	25.5	1990	450	Annealed at
59A(82.0Co-18.0Fe)	236	21.4	1670	480	1000°C and
60A(82.0Co-18.0Fe)	242	23.8	1810	500	Oil Quenched

TABLE 2

SUMMARY OF RESONANT DWELL DAMPING MEASUREMENTS AT 25°C

Sample No. Composition (weight percent)	Resonant Frequency (Hz.)	Dynamical Youngs Modulus ($PSI \times 10^{-6}$)	Peak Stress (PSI)	Loss Factor ($Q^{-1} \times 10^{4}$)	Comments on Test
55A(78.0Co-22.0Fe)	253	25.4	1960	20	All Samples
56A(78.0Co-22.0Fe)	252	26.5	2000	13	Annealed at
61A(90.0Co-10.0Fe)	266	28.2	2170	7	1000°C--Then
62A(90.0Co-10.0Fe)	272	29.8	2270	7	Oil Quenched
63A(65Co-28Fe-7Ni)	244	24.0	1830	28	"
72A(79.0Co-21.0Fe)	249	24.3	1900	19	"
73A(79.0Co-21.0Fe)	264	27.8	2140	10	"
75A(80.0Co-20.0Fe)	249	24.3	1900	24	"
76A(80.0Co-20.0Fe)	251	26.3	1980	274	"
77C(81.0Co-19.0Fe)	232	21.2	2000	11	Machined in 33%
78C(80.5Co-19.5Fe)	248	24.3	2000	12	Cold Worked Condition
79 NIVCO	275	28.3	2000	14	As Received from
79 NIVCO	272	28.2	5000	26	Westinghouse
80C(81.5Co-18.5Fe)	245	23.1	2000	12	Machined--Cold Worked
73B(79.0Co-21.0Fe)	263	27.0	2100	9	Annealed--Water Quenched
77A(81.0Co-19.0Fe)	257	24.8	2000	31	Annealed 1000°C--Then
78A(80.5Co-19.5Fe)	248	24.4	2000	320	Oil Quenched
80A(81.5Co-18.5Fe)	247	24.3	2000	110	"

are near 1000°C.

Table 2 shows additional results for other Co-Fe alloys with compositions in the vicinity of 80 w/o Co-20 w/o Fe which were made and tested in order to establish the effects of composition, structure and degree of cold work on the loss factor. These preliminary results show that the high damping behavior can be reproduced in other alloys but it is eliminated by cold work. This work is proceeding in order to establish the processing limits for obtaining high loss factors.

Table 2 also contains the results of damping tests on NIVCO, which is a commercial alloy developed by Cochardt at Westinghouse (4). It was kindly furnished by Dr. Lou Willertz of Westinghouse Research Laboratories. According to Cochardt's description, NIVCO is 72 w/o Co-23 w/o Ni and the balance titanium and aluminum which are added to provide strength by precipitation hardening. Cochardt reports values of the logarithmic decrement of 0.02 and 0.05 at room temperature for this alloy at shear stresses of 2000 psi and 5000 psi (Figure 1 of Reference 4). Since Q^{-1} is equal to the decrement divided by π, Cochardt's results would correspond to loss factors of 0.007 and 0.017 or 70×10^{-4} and 170×10^{-4} respectively at 25°C and stresses of 2000 psi and 5000 psi. These values are much higher than those shown in Table 2. The values measured in the present tests, i.e. 14×10^{-4} at 2000 psi and 26×10^{-4} at 5000 psi, are five times smaller than Cochardt's results. The main difference is that the frequency of the present measurements at 230-270 Hz is in the audible range while that used by Cochardt was near 1 cycle/sec (1 Hertz).

The results (2) shown in Tables 1 and indicate that loss factors of $Q^{-1} = 500 \times 10^{-4}$ are attainable in the 80 w/o Co-20 w/o Fe alloys which are two to three times higher than observed in Nitinol (i.e. 55 w/o Ni-45 w/o Ti) and fifty times higher than NIVCO. Preliminary results on the 80 w/o Co-20 w/o Fe alloy show almost no change in the audible "ring" (or lack of

"ring") of the alloy at liquid nitrogen or +200°C. Thus it is not anticipated that the Q^{-1} value will decrease significantly in this temperature range.

The other advantages the Co-Fe alloy has in relation to the Ni-Ti alloy are a higher modulus of 25 million psi (Tables 1 and 2) versus 8 million psi and the ease with which the Co-Fe alloy can be fabricated.

In order to evaluate the strength of the 80 w/o Co-20 w/o Fe composition, a set of tensile bars were fabricated of annealed material. Subsequent tests were expanded to test swaged rod. These were compared with tensile results measured for NIVCO (2). The 82 w/o Co-18 w/o Fe and 80 w/o Co-20 w/o Fe alloys show reproducible 0.2 percent offset yield strengths of 17000-18000 psi in the annealed condition. This is the strength level of the samples which exhibited loss factors of $Q^{-1} = 500 \times 10^{-4}$. The yield strength was also measured for samples of the 18.5 w/o Fe, 19 w/o Fe and 19.5 w/o Fe alloys in a cold worked condition following a 33% reduction in diameter by cold swaging. In this condition yield strengths near 70,000 psi were observed (2). Reference to Table 2 shows that these alloys exhibited loss factors of 11 to 14×10^{-4} in the cold worked condition. Annealing raised the loss factor of the 19.5 w/o Fe sample to 320×10^{-4} as shown in Table 2.

Tensile tests on NIVCO produced a 0.2 percent yield strength of 108,900 psi (2) in good agreement with Cochardt's reported value of 110,000 psi (4).

These values of the yield strength were combined with the measured loss factors measured at a stress level of 2000 psi in the range 150 to 250 Hz for NIVCO, 80 w/o Co-20 w/o Fe and 55 w/o Ni-45 w/o Ti are compared in Figure 1. The comparison shows the relatively high damping capacity (and low strength) of the Co-Fe alloy to the other two materials. However, it is likely that this shortcoming can be overcome through alloying. For example, the strength of NIVCO is not due to the properties

of the 72 w/o Co-23 w/o Ni matrix, which is comparable to the 80 w/o Co-20 w/o Fe material. The strength is due to the presence of precipitates formed by the Al and Ti additions. A similar effect can be expected in the Co-Fe alloy. Another possible source of strengthening is additional solid solution hardening which might be effected by addition of nickel. The nickel additions would be controlled so as to maintain the "metastable condition" of the fcc phase. This is illustrated in Figure 9 which shows the ternary Fe-Ni-Co counterpart of Figure 3 calculated on the basis of the thermochemical description published previously (9).

Figure 9 shows the locus of the $\Delta F^{BCC\rightarrow FCC}=0$ and the $\Delta F^{BCC\rightarrow FCC}=+300$ cal/g.at. curves in the Fe-Ni-Co system at 25°C. These alloys should be metastable in the fcc form at 25°C. If they can be fabricated in this state, they may develop high Q^{-1} values comparable to 80 w/o Co-20 w/o Fe and higher yield strengths than the 17,500 psi level exhibited by the 80/20 Co-Fe alloy. Such a series of alloys is currently being fabricated for evaluation. If this effort produces the desired result, it would also have a beneficial effect on the cost of the alloys since it would increase the iron content of the alloy and substitute nickel for cobalt. Both of these composition changes would lower the cost.

In order to proceed with the development of the 80 w/o Co-20 w/o Fe compositions, two separate routes have been pursued. First, fabrication studies on the base composition have been pursued. Second, alloying studies have been carried out in order to evaluate the effects of additions on the strength and damping capacity. All of the measurement techniques employed in these tests are those which have been detailed in earlier reports (1,2).

Three ten-pound heats of the 80 w/o Co-20 w/o Fe alloy have been vacuum melted and cast into two inch diameter moulds. The ingots were subsequently forged to 3/4 inch bars and then (cold) swaged to 1/2 inch rod. Intermediate anneals of 1000°C

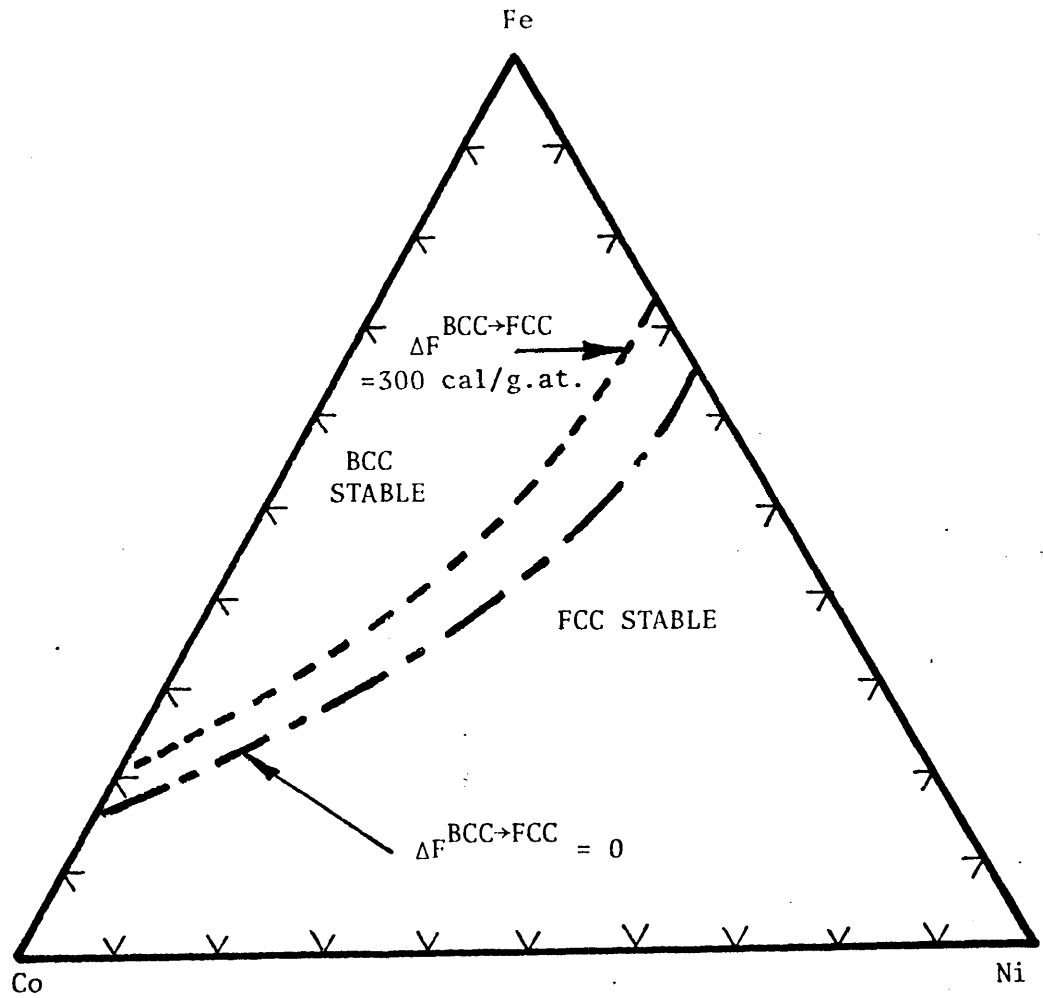

Figure 9 . Calculated Regions of BCC and FCC Stability for Fixed Compositions at 25°C in the Iron-Nickel-Cobalt System.

were employed. The final product was sixty inch long rod. However, it was found that this structure was a mixture of bcc and fcc phases (see earlier discussion) and the rod "rang" when struck, indicating poor damping. However, the high damping characteristics were readily restored by proper heat treatment above 1000°C followed by air cooling. The x-ray analysis of the material disclosed a fully austenitic (fcc) structure and the high damping characteristic of the rod was regenerated.

A second demonstration of the ease with which the 80 w/o Co-20 w/o Fe alloy can be fabricated was the reduction of as-cast 1/2 inch thick slab to 50 mil foil. This was carried out in a series of 20% reductions with intermediate anneals. The reductions were quite moderate and the ease with which they were made indicates that even larger reductions could be successfully carried out. This would certainly appear to be possible if the reductions were carried out by hot rolling. The final treatment of the fifty mil foil consisted of a 1000°C for 30 minutes which yielded soft foil which "rang like lead."

These results indicate that the 80 w/o Co-20 w/o Fe alloy can be readily formed if it is in the fcc condition. Moreover it can be heat treated to yield this structure quite readily. Although it has been established that the two phase (fcc+bcc) structure does not exhibit outstanding damping characteristics, it is probable that rather high strengths could be attained with this structure if it were attained by formation of an ordered bcc phase. This alloy (80 w/o Co-20 w/o Fe) could be readily formed in the fcc structure (as demonstrated above) and then aged to high strength by ordering the bcc phase. In fact, small carbon additions might even be incorporated into such a structure to enhance the strength by conferring some tetragonality into the bcc phase in analogy with ferrous martensites.

Before turning to the alloying studies conducted on the 80 w/o Co-20 w/o Fe alloy it is useful to recount the temperature dependent studies undertaken to establish the data shown in Figure

2. The tests were conducted under the direction of Dr. John Heine of Bolt Beranek and Newman using the techniques detailed earlier (1,2).

Figures 10 and 11 show loss factor versus temperature curves for samples of a 80.5 w/o Co-19.5 w/o Fe and 81.5 w/o Co-18.5 w/o Fe alloy between -60°C and +80°C. Additional samples which were tested between 25°C and 130°C yield the results shown in Figure 2.

In order to obtain an additional set of data on a high damping alloy which is generally available, a sample of Incramute was obtained from Mr. Eugene Thiele of the Copper Development Association Inc. A square plate 5 1/2 inches x 5 1/2 inches x 1/4 inch thick was obtained in the heat treated condition designed to yield maximum damping. This plate was employed to fabricate resonance dwell damping bars (1,2) and tensile bars. Figure 12 shows the results of the damping measurements conducted on the Incramute (55 w/o Co-43 w/o Mn-2 w/o Al) alloy between -60°C and 100°C. Tensile tests conducted at 25°C resulted in a 0.2% offset yield strength of 45,300 psi. These data are shown in Figures 1 and 2.

It is interesting to note that the copper-manganese alloy system, upon which Incramute and several other commercial damping alloys are based was predicted to have a metastable fcc miscibility gap in 1969 (14). Recent experimental studies by Vitek and Warlimont and by Ye. Z. Vintaykin and coworkers (16) have verified this prediction and Figure 13 shows that the metastable miscibility gap in the fcc phase of this system provides the basis for attaining high damping in Incramute and other Cu-Mn alloys via heat treatment.

The second phase of the study of damping in the 80 w/o Co-20 w/o Fe alloy currently under investigation is the evaluation of alloying additions on damping and strength. These activities were initiated during the past three months and have thus far demonstrated that substantial increases in strength can be obtained. However, the optimum "trade off composition" has not yet

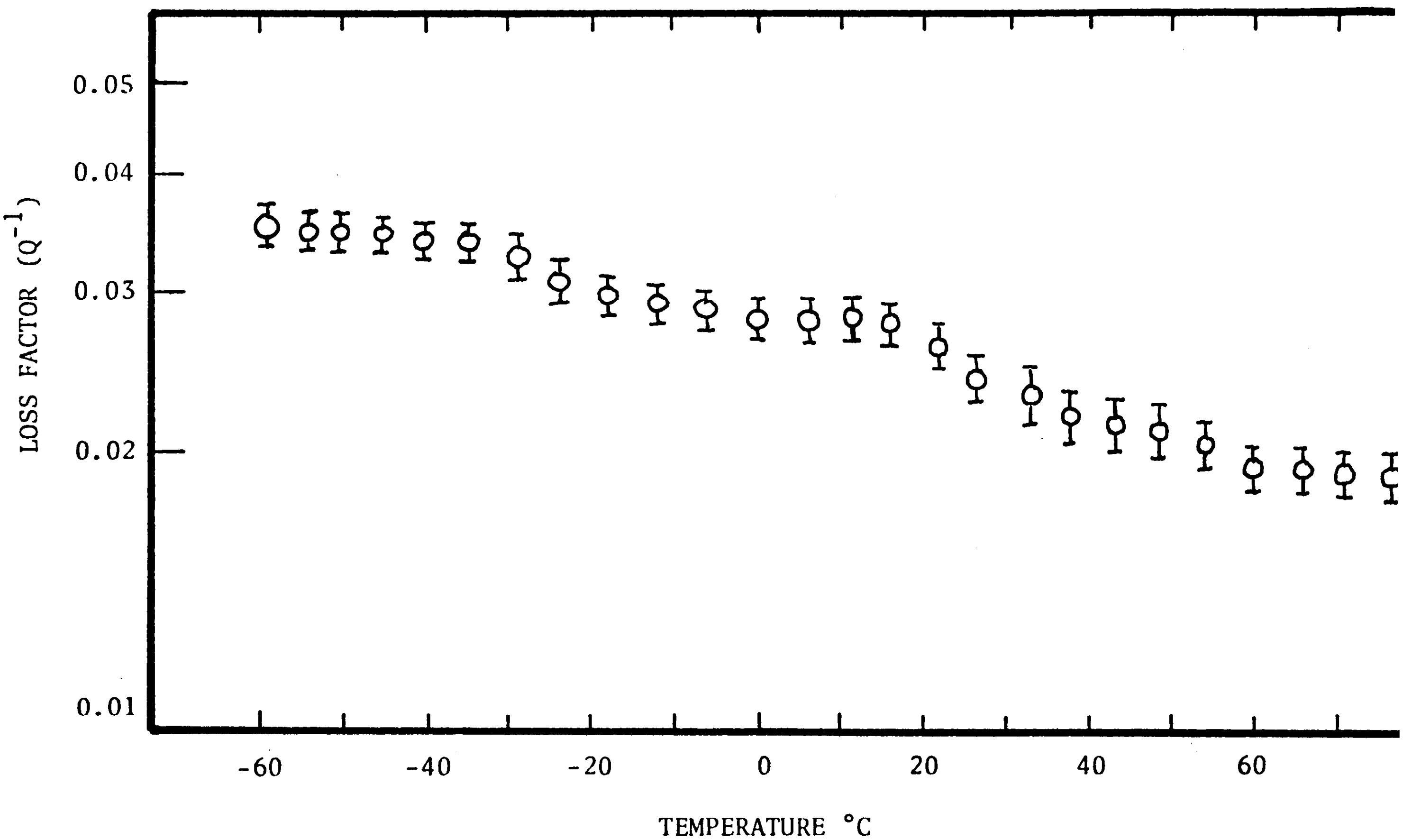

Figure 10. Loss Factor vs. Temperature Curve for a Sample of 80.5 w/o Co-19.5 w/o Fe measured at 240-250 Hertz and a stress of 2000 psi. The dynamical Young's Modulus measured over the same temperature range varied from 24 million psi at -60°C to 23 million psi at +80°C. The sample was annealed at 1000°C and air cooled.

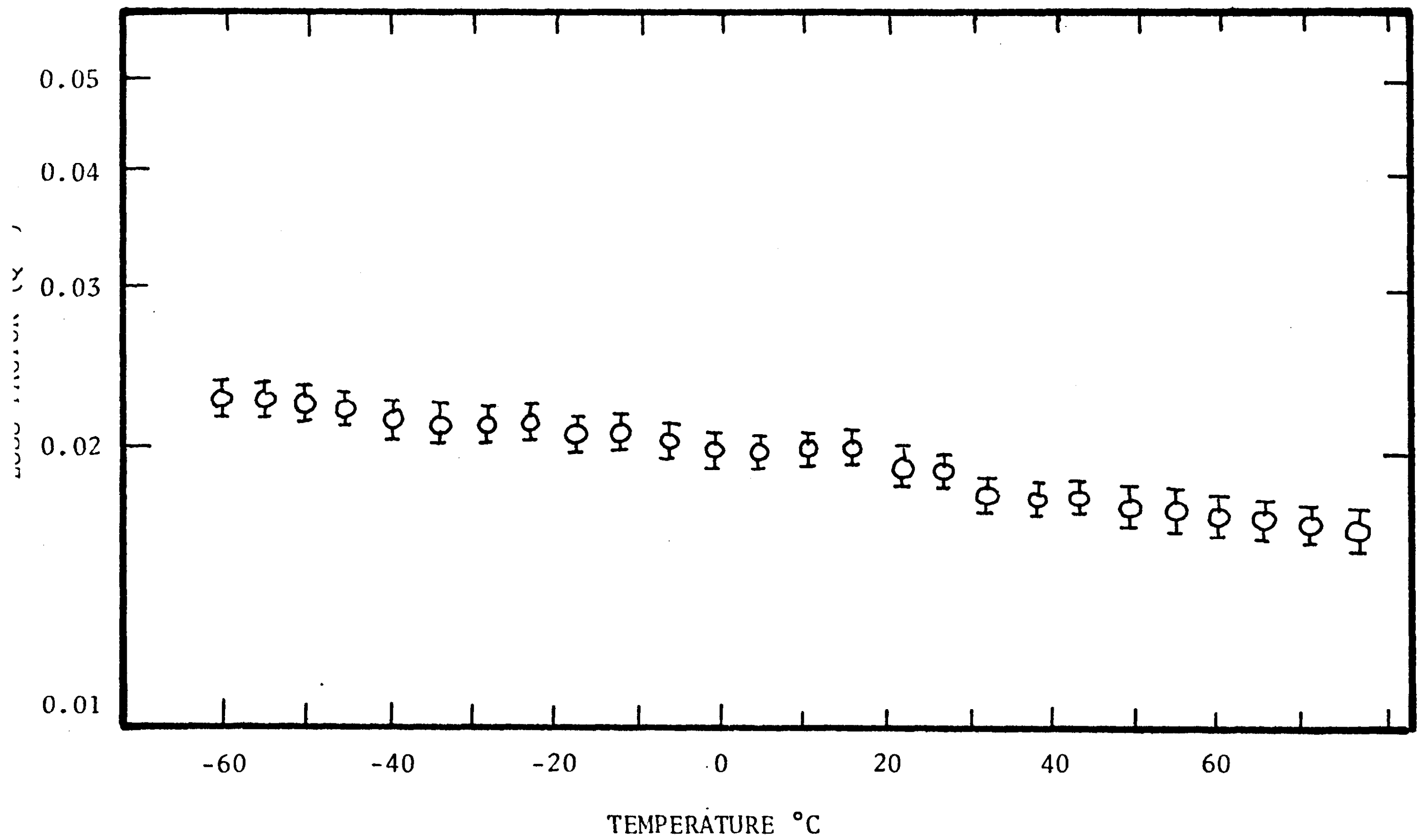

Figure 11. Loss Factor vs. Temperature Curve for a Sample of 81.5 w/o Co-18.5 w/o Fe measured at 240-250 Hertz and a stress of 2000 psi. The dynamical Young's Modulus measured over the same temperature range varied from 24 million psi at -60°C to 23 million psi at +80°C. The sample was annealed at 1000°C and air cooled.

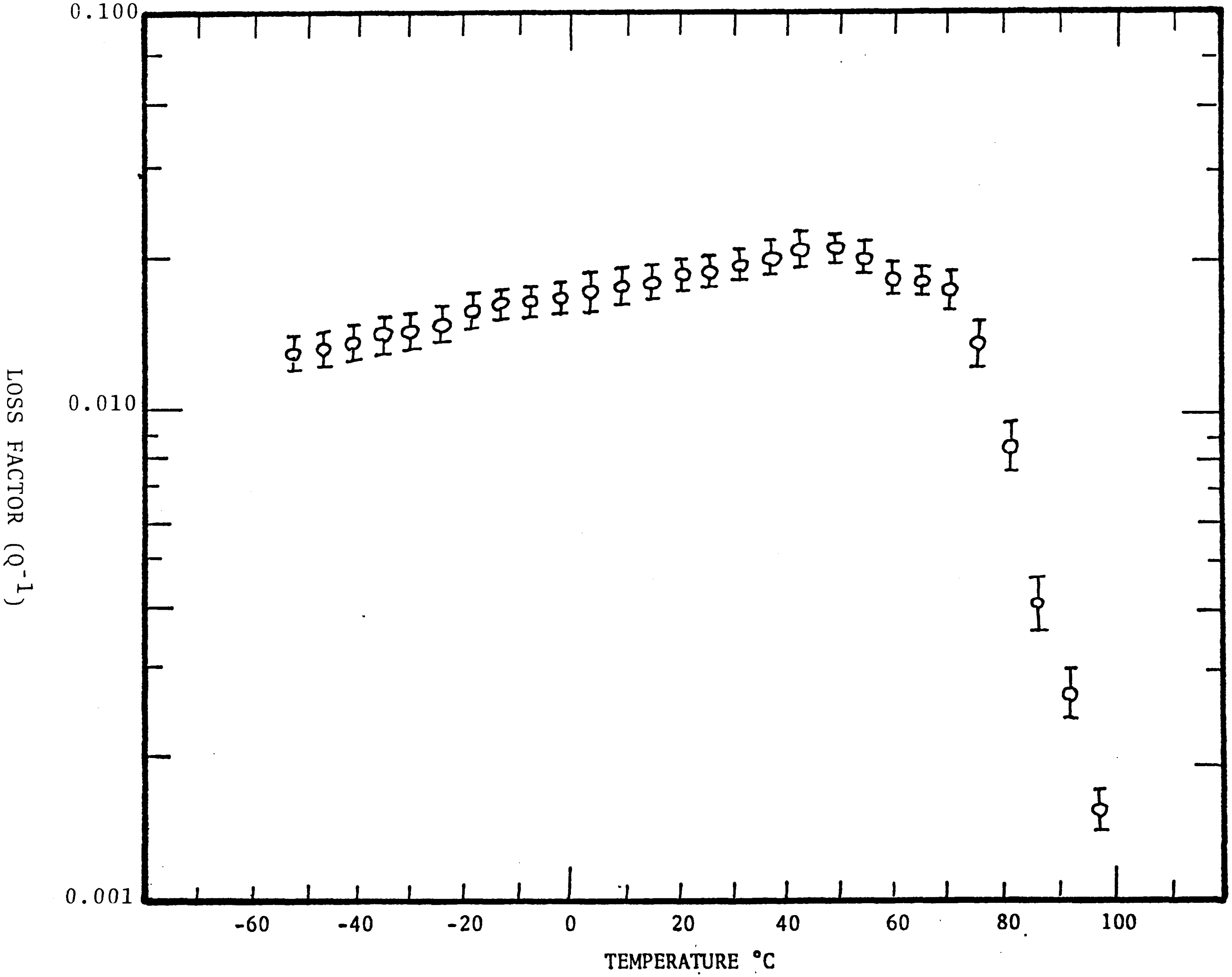

Figure 12. Loss Factor vs. Temperature for a Sample of Incramute I (Nominal Composition 55 w/o Cu-43 w/o Mn-2 w/o Al) heat treated for maximum damping characteristics

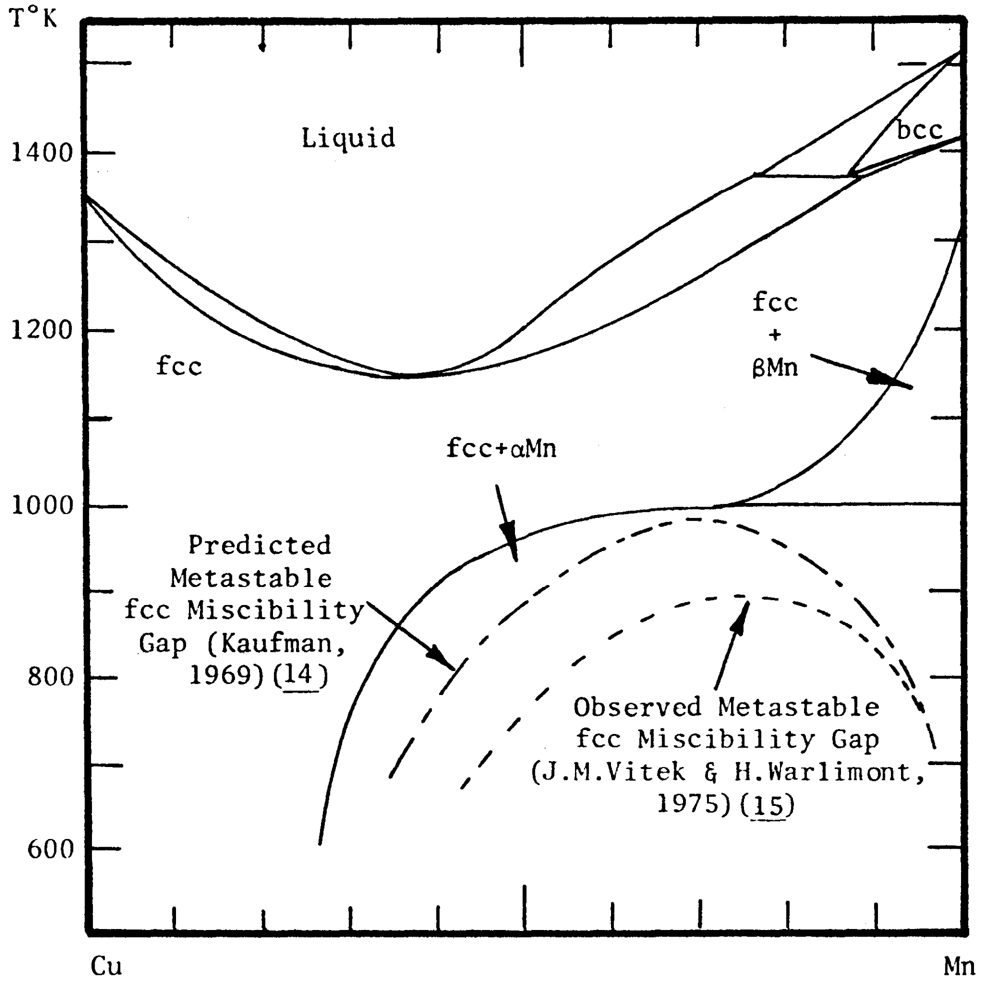

Figure 13. Predicted (14) and Observed (15) Metastable Miscibility Gaps in the Cu-Mn System.

been identified.

Table 3 shows the preliminary results which have been obtained. This compilation shows results of alloys synthesis, fabrication damping, and tensile tests on eight alloys based on the Co-Fe composition with substanital additions of nickel or small additions of manganese or aluminum. These results were employed in construction the bar graph shown in Figure 1.

The results obtained thus far indicate that the additions of nickel do not offer any substantial improvement in strength. However, very substantial increases in strength have been attained with aluminum and manganese. These improvements have been accompanied by a decrease in damping capacity. Nevertheless it is interesting to note that sample number 102 (76 w/o Co-19 w/o Fe-5 w/o Mn) exhibited twice the damping capacity of NIVCO at a comparable strength level (see Figure 1) while sample 99 (76 w/o Co-18 w/o Fe-5 w/o Al) exhibited a yield strength of 182,000 psi versus 110,000 psi for NIVCO at the same level of damping capacity which NIVCO exhibits (2).

Table 4 summarizes the results of damping and mechanical property measurements conducted on a series of cobalt-iron and cobalt-iron base alloys to which additions of manganese, chromium and aluminum have been made. In each case, evaluation of the damping and yield strength have been made on samples which were cold worked by rolling (to 10% reduction in thickness) as well as on companion samples annealed at 1000°C and air cooled.

The results obtained with sample composition 111 and 112 indicate a very abrupt change in behavior when the aluminum content is increased from 2.5 w/o (i.e., samples 97 and 98 in Table 3) to 3 w/o (i.e., samples 111 and 112 in Table 4). As was noted previously (2) aluminum additions result in subtantial increases in the tensile strength of the cobalt-iron which are accompanied by similar decreases in the loss factor. The compositions corresponding to 111 and 112 represented an attempt

TABLE 3

SUMMARY OF 0.2 PERCENT OFFSET YIELD STRENGTH AND
RESONANT DWELL DAMPING MEASUREMENTS AT 25° (Peak Stress 2000 PSI)
(ALL SAMPLES WERE MACHINED THEN ANNEALED
AT 1000°C AND AIR COOLED)

Sample No. Composition (weight percent)	Resonant Frequency (Hz.)	Dynamical Youngs Modulus (PSI x 10^{-6})	Loss Factor	0.2 Percent Offset Yield Strength (PSI)
85-(60Co-28Fe-12Ni)	243	24.0	0.0026	23100
86-(60Co-28Fe-12Ni)	246	24.6	0.0056	32400*
87-(50Co-32Fe-18Ni)	243	24.0	0.0026	30000
88-(40Co-38Fe-22Ni)	225	20.6	0.0016	29800
94-(72Co-18Fe-10Mn)	264	28.3	0.0011	53700
95-(72Co-18Fe-10Mn)	275	30.7	0.0008	87700*
97-(78.5Co-19Fe-2.5Aℓ)	255	26.4	0.0015	25000
98-(78.5Co-19Fe-2.5Aℓ)	240	23.4	0.0029	29900*
99-(76Co-18Fe-6Al)	273	30.3	0.0013	182000
100-(76Co-18Fe-6Al)	268	29.2	0.0011	157000*
101-(76Co-19Fe-5Mn)	262	27.9	0.0010	83800
102-(76Co-19Fe-5Mn)	264	28.3	0.0027	105700*
103-(77Co-19Fe-4Al)	271	30.1	0.0015	145000
104-(77Co-19Fe-4Al)	269	29.4	0.0011	152000*

*Cold Worked

TABLE 4

SUMMARY OF 0.2 PERCENT OFFSET YIELD STRENGTH AND RESONANT DWELL DAMPING MEASUREMENTS AT 25°C (Peak Stress 2000 PSI) (SAMPLES WERE MACHINED IN THE COLD WORKED CONDITION AND TESTED DIRECTLY OR ANNEALED AT 800°C or 1000°C (AN800, AN1000) AND AIR COOLED BEFORE TESTING)

Sample No. Composition (weight percent)	Condition	Resonant Frequency (Hz.)	Dynamical Young's Modulus (PSI x 10^{-6})	Loss Factor	0.2 Percent Offset Yield Strength (PSI)
106A-(78Co-20Fe-2Mn)	AN1000	248	24.2	0.0400	18000
106B-(78Co-20Fe-2Mn)	CW	250	24.3	0.0020	45000
107 -(72Co-18Fe-10Cr)	AN1000	238	23.8	0.0078	20000
108 -(72Co-18Fe-10Cr)	CW	237	23.8	0.0040	26000
109 -(80Co-20Fe)	AN1000	243	24.0	0.0400	17400
110 -(80Co-20Fe)	CW	249	24.3	0.0090	25000
111 -(77Co-19Fe-3Aℓ)	AN1000	267	27.9	0.0009	78000
112 -(77Co-19Fe-3Aℓ)	CW	270	28.5	0.0008	113000
113 -(77.2Co-19.2Fe-3.6Mn)	AN1000	247	24.2	0.0270	18000
114 -(77.2Co-19.2Fe-3.6Mn)	CW	247	24.2	0.0042	24800
115 -(76.4Co-19.2Fe-4.4Mn)	AN1000	254	26.2	0.0009	67000
116 -(76.4Co-19.2Fe-4.4Mn)	CW	255	26.3	0.0008	106000

to effect an increase in strength without experiencing a decrease in damping by operating at a composition close to that of samples 97 and 98. Unfortunately however, the desired increase in strength (to 78,000 psi) in the annealed condition was accompanied by a drop in damping.

Although the studies of aluminum additions have been disappointing in the sense that an alloy combining high damping and high strength has not been identified, the observation that small additions of aluminum result in substantial strength and corresponding increases in hardness (RB 30 for 0 w/o Aℓ to RC 44 for 4 w/o Al) in the annealed condition may be of practical value. In particular, in the event an application demanding high damping and high hardness should present itself, it might be possible to "alluminize" an 80 Co- 20 Fe alloy and obtain a wear resistant surface on a component with a high loss factor.

The results obtained with additions of chromium to the base cobalt-iron composition as disclosed by sample composition 107 and 108 suggest modest increases in strength accompanied by subtantial decreases in loss factor. Accordingly further studies of chromium additions have been curtailed.

As indicated in the previous report (3), additions of manganese were observed to provide an avenue for increasing the strength of the cobalt-iron alloys. Table 4 summarizes the results obtained on an additional series of cobalt-manganese alloys investigated during the present period. These results, which are shown graphically in Figure 14 suggest that a "trade-off" between strength and damping can be optimized at about 4 w/o Mn. An alloy of this composition is currently being fabricated.

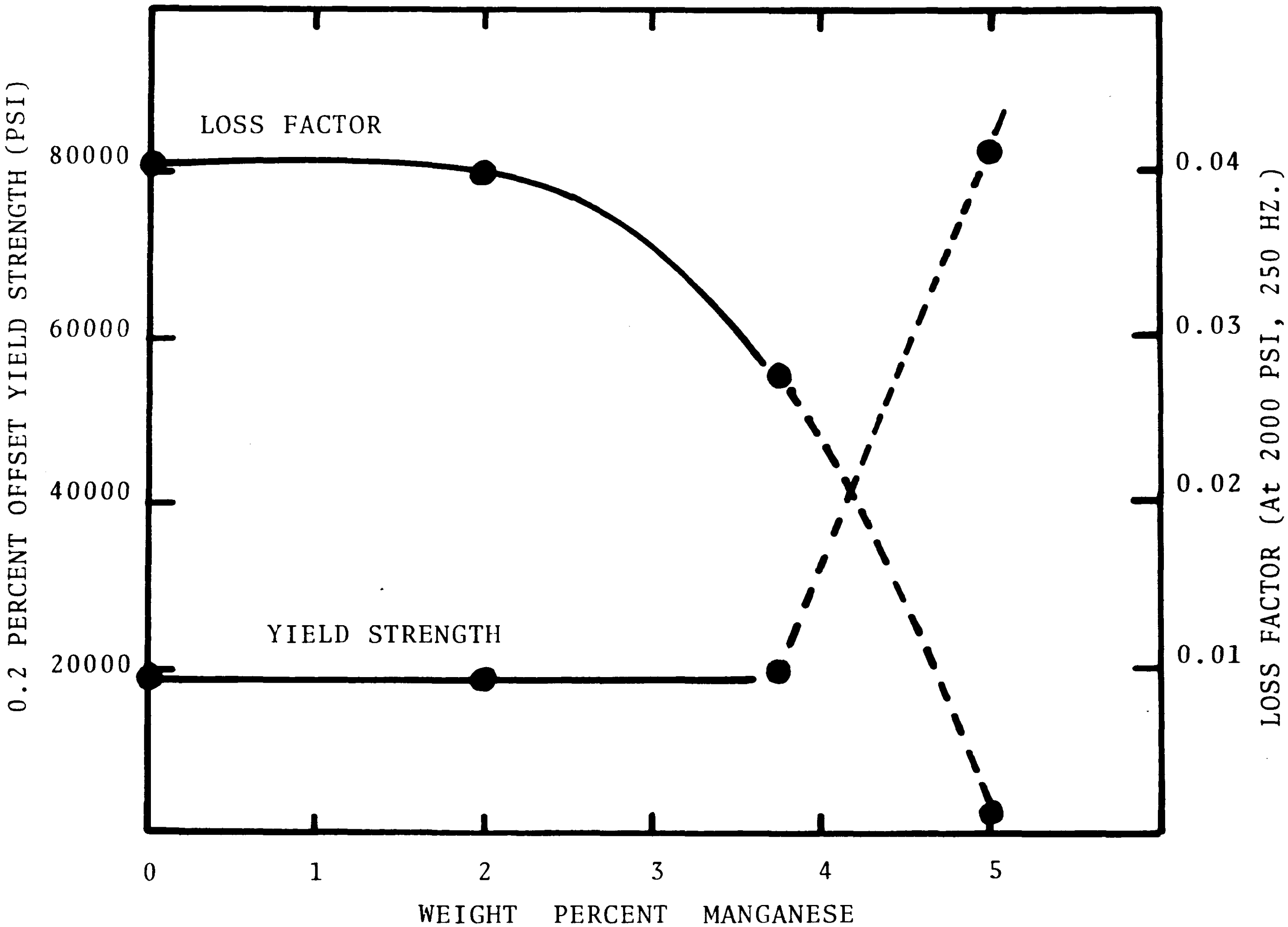

Figure 14. Loss Factor and 0.2 Percent Offset Yield Strength vs Manganese Content for a series of Cobalt-Iron-Manganese Alloys.

III. INVESTIGATION OF IRON - CHROMIUM ALLOYS FOR APPLICATION AS HIGH DAMPING STRUCTURAL MATERIALS

One of the main short comings of the cobalt - base alloys as potential structural materials with high damping capacity is the cost per pound. Since cobalt is currently in the \$3 to \$4 per pound range, the finished cost for wrought cobalt parts can be as high as \$5 per pound even if large quantity use were projected. In order to evaluate the potentials offered by iron base alloys as damping materials for structural applications at a lower cost per pound (i.e., \$0.50/lb.) several iron - chromium base alloys have been examined.

This work was stimulated by the reports distributed by Toshiba Electric Co. (17) on a proprietary Fe-Cr-Al alloy and the existence of a miscribility gap in the Fe - Cr system shown in Figure 15 just as there is in the Cu - Mn case shown in Figure 13. Although the mechanism responsible for the damping in Fe - Cr - Aℓ has not been established, the miscibility gap in both systems is a common feature.

Accordingly, samples of Fe - Cr - Aℓ alloys and Fe - Cr - C alloys corresponding to several commercial steels were prepared and tested. The results are summarized for Samples 117-125 shown in Table 5, and Figures 16 and 17. It was found that the optimum temperature for heat treatment was 800°C (1073°K). Heat treatment at higher temperatures (i.e., above 1000°C) (1273°K) within the gamma loop leads to low damping. This may be related to the transformation structure in the resulting bcc phase following the fcc→bcc transition on cooling. Heat treatment at 600°C (873°K) did not yield results which were as satisfactory as those obtained at 800°C.

Reference to Table 5 shows that attractive damping capacity and yield strength characteristics can be obtained in the 85 w/o Fe - 12 w/o Cr - 3 w/o Aℓ alloy as well as the 86 w/o Fe - 14 w/o Cr - 0.05 w/o C alloy. The latter corresponds in

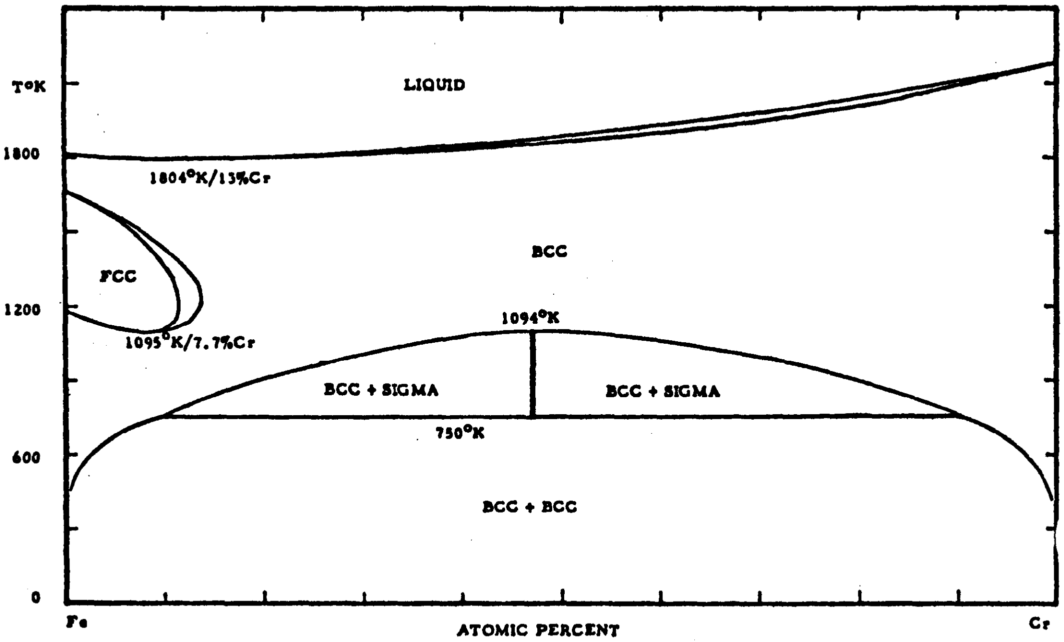

Figure 15. Iron-Chromium Phase Diagram.

TABLE 5

SUMMARY OF 0.2 PERCENT OFFSET YIELD STRENGTH AND RESONANT DWELL DAMPING MEASUREMENTS AT 25°C (Peak Stress 2000 PSI) (SAMPLES WERE MACHINED IN THE COLD WORKED CONDITION AND TESTED DIRECTLY OR ANNEALED AT 800°C OR 1000°C (AN800, AN1000) AND AIR COOLED BEFORE TESTING)

Sample No. Composition (weight percent)	Condition	Resonant Frequency (Hz.)	Dynamical Young's Modulus (PSI x 10^{-6})	Loss Factor	0.2 Percent Offset Yield Strength (PSI)
117-(85Fe-12Cr-3Aℓ)	AN800	258	26.5	0.0360	37900
118-(85Fe-12Cr-3Aℓ)	CW	260	26.6	0.0030	42000
119-(85Fe-12Cr-3Aℓ)	AN600	256	26.4	0.0030	32500
120-(85Fe-12Cr-3Aℓ)	CW	257	26.5	0.0030	39000
121-(88Fe-12Cr-0.12C)	AN800	290	31.8	0.0028	40000
122-(88Fe-12Cr-0.12C)	CW	292	32.2	0.0010	49000
123-(88Fe-12Cr-0.08C)	AN800	288	31.3	0.0042	54000
124-(88Fe-12Cr-0.08C)	CW	290	31.8	0.0015	84000
125-(86Fe-14Cr-0.05C)	AN800	292	32.2	0.0180	42000
126-(86Fe-14Cr-0.05C)	CW	303	34.3	0.0008	49000
TESTED AT A PEAK STRESS OF 500 PSI					
109-(80Co-20Fe)	AN1000	250	24.3	0.0202	17400
TESTED IN A MAGNETIC FIELD UNDER CONDITIONS OF SATURATION					
109-(80Co-20Fe)	AN1000	243	24.0	0.0170	17400
117-(85Fe-12Cr-3Aℓ)	AN800	258	26.5	0.0230	37900
125-(87Fe-13Cr)	AN800	294	32.6	0.0065	42000

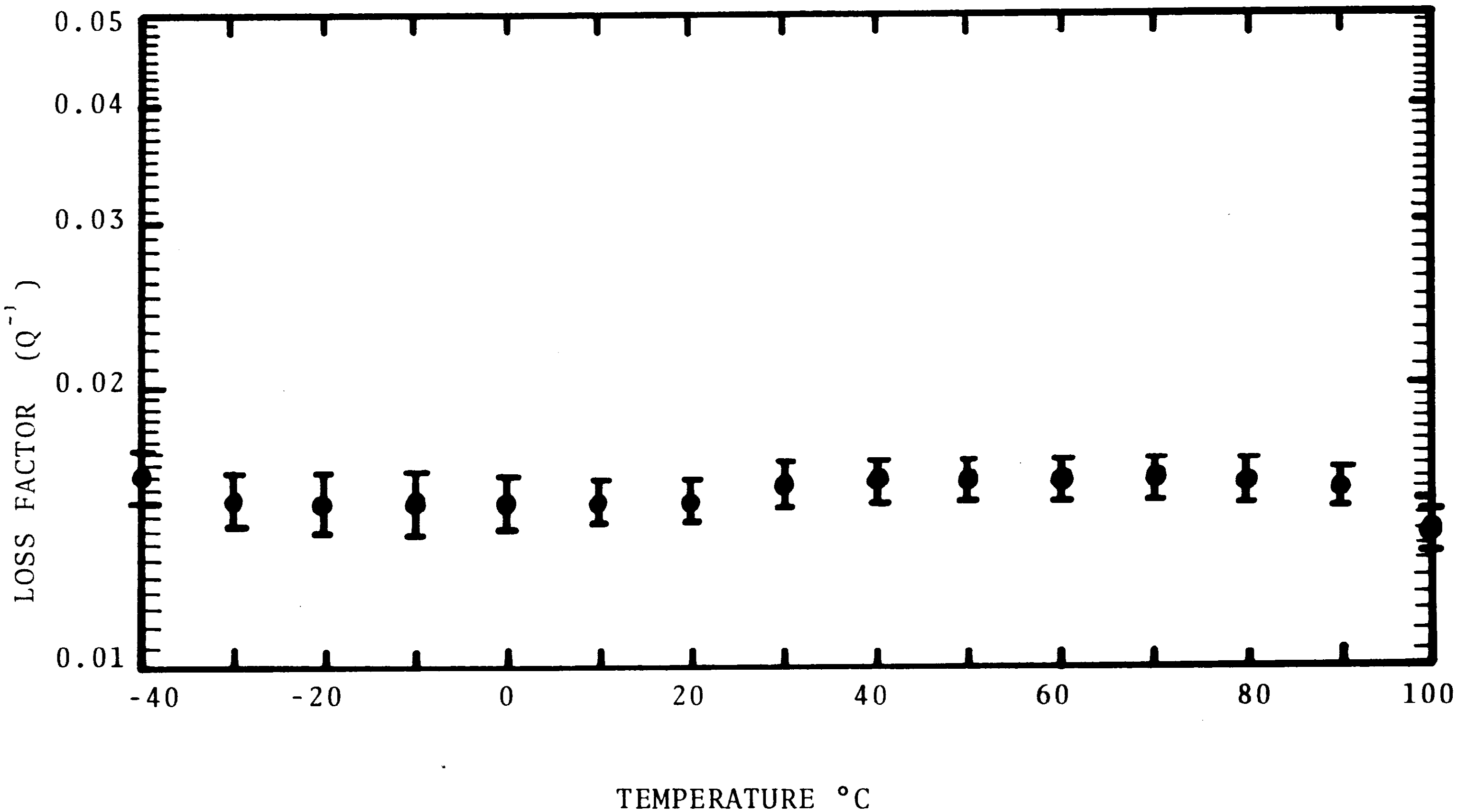

Figure 16. Loss Factor vs. Temperature Curve for a Sample of 85 w/o Fe - 14 w/o Cr - 0.05 w/o C Measured at 290 - 300 Hertz and a Stress of 2000 psi.

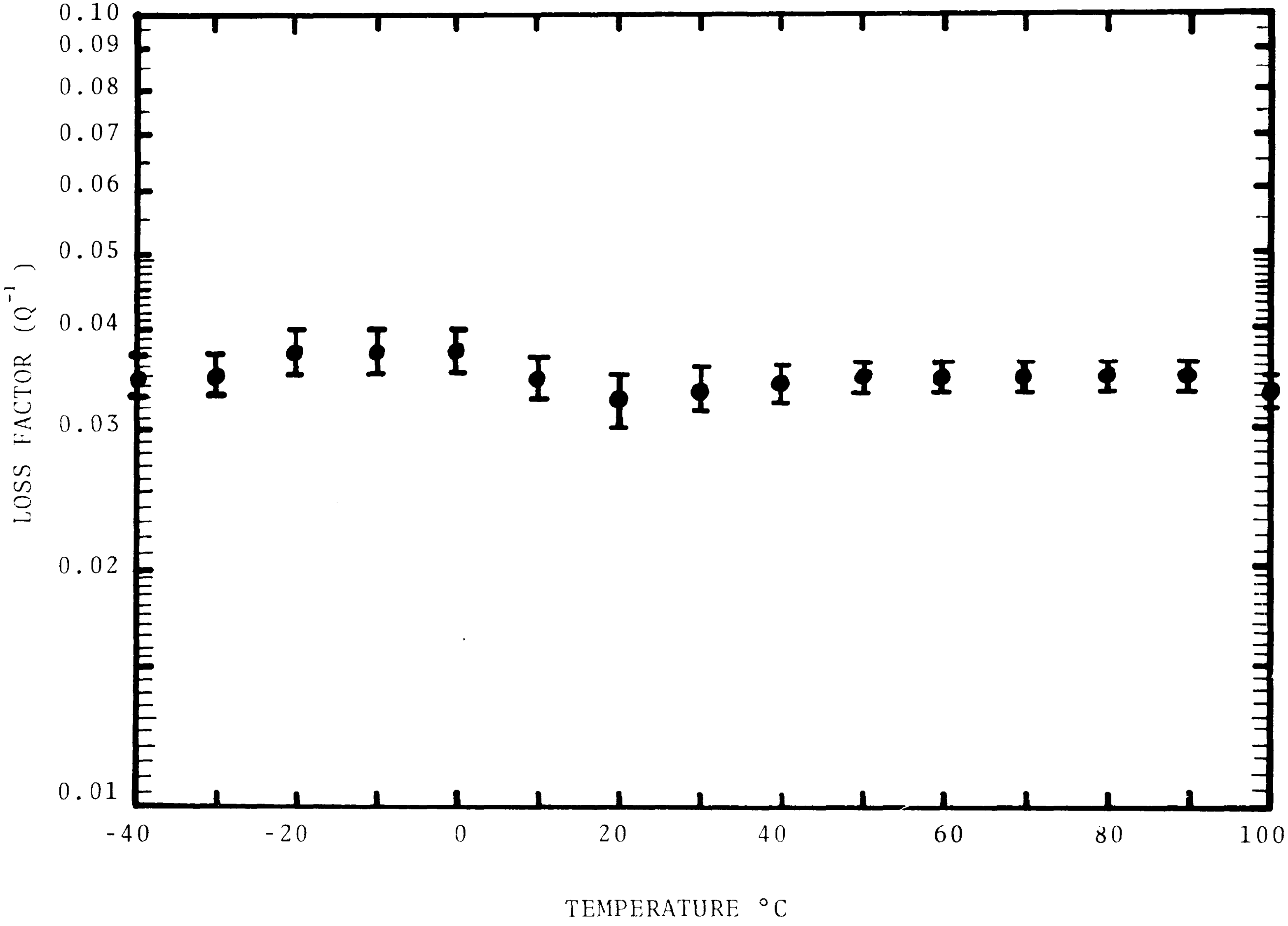

Figure 17. Loss Factor vs. Temperature Curve for a Sample of 85 w/o Fe - 12 w/o Cr - 3 w/o Aℓ measured at 250-260 Hertz and a Stress of 2000 psi.

in composition to type 405 stainless steel (i.e., samples 125, 126). Samples 121, 122, 123 and 124 correspond to types 410 and 403 stainless steel respectively. The results indicate that combinations of 4000 psi yield strength, loss factors of 0.02 - 0.04, good corrosion resistance and a cost per pound of $0.50 - $0.80/lb., can readily be attained in alloys of the iron - chromium system. However, optimization of properties will undoubtedly depend on third alloying element additions as well as heat treatment as indicated by Table 5.

Figures 16 and 17 indicate that the damping is insensitive to changes in temperature up to 100 °C. These results were obtained on samples 125 and 111 which are shown in Figures 16 and 17 respectively. The results of similar studies at Toshiba Electric suggests that the loss factor is insensitive to temperature up to 300°C. Table 5 also contains some results on the 80 w/o Co - 20 W/o Fe alloy at a lower stress (500 psi) as well as the 80 w/o Co-20 w/o Fe and the iron - chromium alloys in a saturating field.

The former result at 500 psi indicates a loss factor of about 2% for the Co - Fe alloys as compared with a loss factor of 4% for this alloy at 2000 psi. This is in keeping with the general finding that the loss factor is proportional to stress to the one half power.

Measurement of the loss factor at 2000 psi in a saturating magnetic field indicated a decrease in the loss factors of the cobalt-iron alloy and the iron-chromium base alloys. These results indicate that some of the damping behavior is of magnetic origin. Nevertheless, the measured values of the loss factors in a saturating field remained high enough to indicate that other mechanisms may be contributing to the damping behavior in these alloys.

IV. CONSIDERATION OF POTENTIAL APPLICATIONS OF HIGH DAMPING ALLOYS.

A survey of potential applications of high damping alloys to problems of noise and vibration control was conducted in order to examine problem areas in military and civilian systems, which could benefit from advances in damping materials technology. Tables 6 and 7 list some of the results of this survey. In this listing, general items and specific applications are noted. Each entry is also accompanied by material properties which are required in addition to damping for the specific application. For the cases listed in Tables 6 and 7, high damping characteristics would be a desirable feature of the metallic component since add-on noise or vibration treatments are inappropriate or too expensive.

In the basis of this survey, it appears that three potential application merit particular consideration. These are ship propellers, body panels of military reconnaissance vehicles, engine oil pans, and valve covers. In each case, improvement in the damping properties may be expected to lead to significant reductions of radiated noise and hence, in acoustic detectibility an/or tolerance. In the former application, damped propellers have proven to be effective. The availability of high damping alloys with a known loss factor could lead to propellers with better reliability allowing design for optimized thrust at a lower cost. The benefits of additional damping in materials used for body panels of military reconnaissance vehicles, and for engine components have not yet been quantitatively determined. However, a recently completed model study (18) has demonstrated its significance. Subsequent parts of this section discuss these principal areas of application.

1.0 High Damping Materials For Military Ship Propellers

High damping in some propellers of military vessels is currently acheived through a complicated design involving

TABLE 6

POTENTIAL APPLICATIONS OF HIGH DAMPING ALLOYS IN NOISE CONTROL

ITEM	APPLICATION	PRIMARY PROPERTIES
Propellors	Military Ship Propulsion	Corrosion Resistance Surface Fatigue Strength
Gears	Ship & Helicopter Power Train	Fatigue Strength Stiffne
Hull Plating and Engine Oil Pans and Valve Covers	Military Reconnaissance Vehicles	Formability
Mufflers and Ducts	Air Compressors	Fatigue Strength
Damped Springs & Suspensions	Land Vehicles	Fatigue Strength
Perforated Plates for Test Cells	Engine Test Cells	High Temperature
Cams and Cam Followers Relays & Ratchets	Machinery & Control Systems	Fatigue Strength Stiffness
Machinery Stops	Production Machines Automatic Weapons	Fatigue Strength Stiffness
Saw Blades	Fabrication Machinery	Fatigue Strength Abrasions Resistance
Impact Bits	Jack Hammers	Abrasions Resistance Fatigue
Grinders & Pelletizers	Material Preprocessing (e.g., plastics)	Abrasions Resistance
Wheel Squeal	Rail Vehicle Wheels and Retarders	Abrasion Resistance
Material Transfer & Handling	Food & Chemical Processing	Abrasion Resistance Resistance to Chemicals Formability

TABLE 7

POTENTIAL APPLICATIONS OF HIGH DAMPING ALLOYS IN VIBRATION AND FATIGUE CONTROL

ITEM	APPLICATION	PRIMARY PROPERTIES
VIBRATION CONTROL		
Engine Crank Shafts	Piston Engines	Fatigue
Electronic Chasses	Vehicle-Borne Electronics	Fatigue
Machine Tool Holders	Production Machinery	Strength
Machinery Stops	Production Machinery Automatic Weapons	Stiffness Fatigue Strength
Cam & Cam Followers, Rely & Ratchet Devices	Machinery & Control Systems (e.g., high speed printers)	Fatigue Strength Stiffness
FATIGUE CONTROL		
Turbine Blades	Turbo Machinery	High Temperature Strength Low Density
Aircraft Components	Surface Structures and Equipment Near Engines and Armaments	Fatigue Strength
Light Bulb Filaments	Bulbs for all Vehicles	Luminescence Electrical Resistance High temperature Fatigue Strength
Nuclear Reactor Components	Gas Cooled Reactors	Compatibility with Reactor Environment

composite materials. The levels of damping achieved by this route are satisfactory. Loss factors of the propellers as a vibratory system are not available at this time. However, materials with loss factors of 4% under the required dynamic and static stresses are serious candidates for propeller materials if costs are reasonable and, if other important materials properties are achieved. In particular, any materials which is considered for use must generally meet the requirements of MIL-B-21230, which are as follows: Fatigue Life: 10^8 cycles in salt water at a 9000 psi mean stress, 2700 psi alternating stress. A yield strength of 35000 psi is required and the material must be castable, easily welded, and capable of withstanding chipping and grinding. In addition, it must be machinable so that 63 micro-inch finish can be acheived. The alloy must be resistant to stress corrosion, cavitation corrosion, and fatigue for long periods of exposure.

Salt water fatigue tests are performed at NSRDC Annapolis. The specimen size required is a 10.5 to 12 inch long bar with a 1" circular cross section. The speciman is cantilevered and point loaded at the free end to produce a peak stress which is increased to 9-13000 psi. Salt water is applied to a 3 inch long section of the bar at the clamped end and a dynamic stress of 2700 psi around the mean is applied for 10^8 cycles at a rate of 1450 cycles perminute. Thus, this test requires approximately fifty days of continous testing. Typically five tests are run, and one control test is run in air. Cavitation corrosion tests are performed by NSROC Annapolis. The test sample required is a 6" x 6" x 1/8" plate.

2. High Damping Material For Armoured Personnel Carriers.

Recent measurements performed by Bolt, Beranek and Newman Inc., under contract No. DAAE07-74-C-0002 on a 1/6 scale dynamic model of an armoured personnel carrier (APC) indicated

that the exterior and interior noise of an APC depends significantly on the damping of the APC hull. The 1/6 scale dynamic model, which is shown in Figures 18-21 has been instrumented in order to provide detailed measurements of interior and exterior radiated noise (18). Although no quantitative measurements were made, it was found that the addition of damping treatment greatly reduced the observed noise.

A high damping metal or alloy could make a contribution here, if it can meet all other requirements for APC hull panels. Foremost, there is "ballistic penetration resistance". Since current hulls are made of 5083 aluminum, any new material would have to provide comparable performance per unit weight. Requirements for hull materials properties are contained in MIL-A-46027 and its Ballistics Acceptance Supplement.

It appears that specific goals for materials loss factors can be determined using the above mentioned scale model. A measurement program could be initiated to determine radiated noise reduction as a function of hull panel loss factor. An upper boundary on the useful loss factor will exist, since further damping to reduce noise is not useful once the pause noise contribution is approximately the same as that from other noise sources (e.g., the track). Panels with add-on damping treatment could be utilized in this test.

Alternatively, the alloys discussed in Sections I and II could be tested directly on the 1/6 scale model to carry out comparative measurements of radiated power. In order to carry out such a test, eleven plates of the alloys must be fabricated and machined to fit the model. Comparative measurements of the damping alloys vs. aluminum, for both interior and exterior noise could then be made for the model over a range of speeds. The specific plate sizes in 1/4" thick gauge are 11" x 18", 10" x 16", 16" x17", 9" x 16", 4" x 11", 5" x 21" (2) and 6" x 21" (2). Finally, two plates measuring 1/10" x 4" x 21" are required.

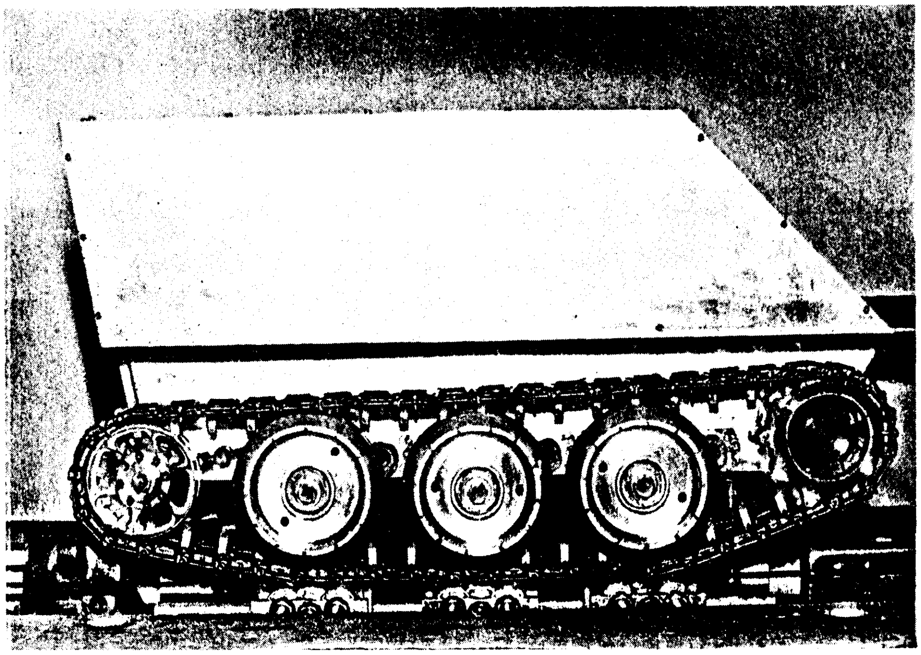

Figure 18. Side View of 1/6 Scale Model of Armoured Personnel Carrier (Courtesy of Bolt, Beranek, Newman Contract DAAE07-74-C-0022).

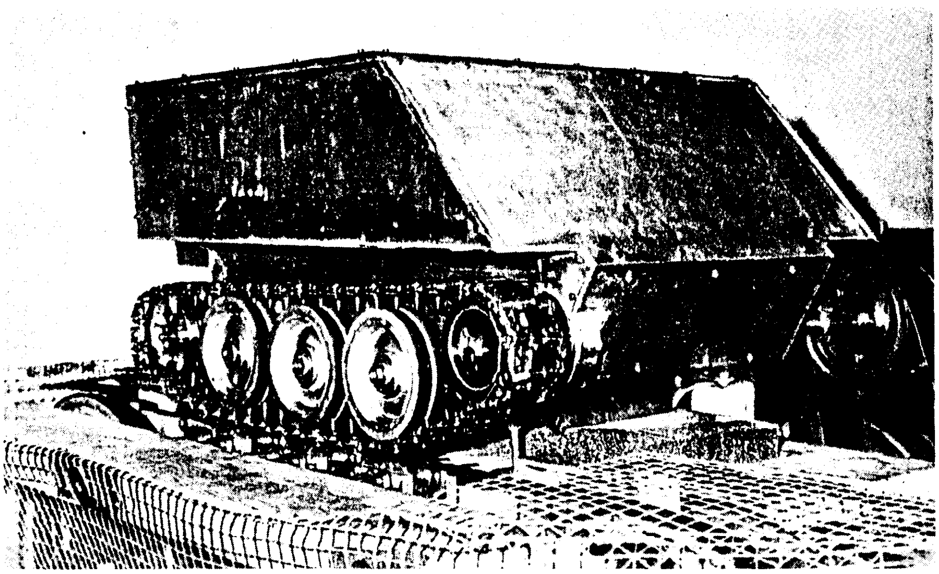

Figure 19. Front View of 1/6 Scale Dynamic Model.

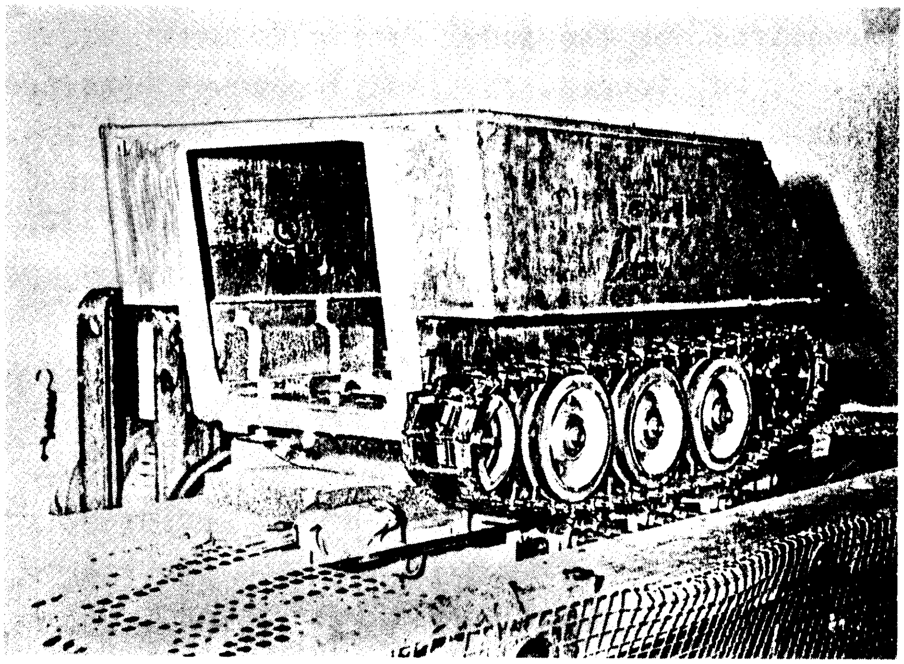

Figure 20. Rear View of 1/6 Scale Dynamic Model of Armoured Personnel Carrier (Courtesy of Bolt, Beranek, Newman Contract DAAE07-74-C-002).

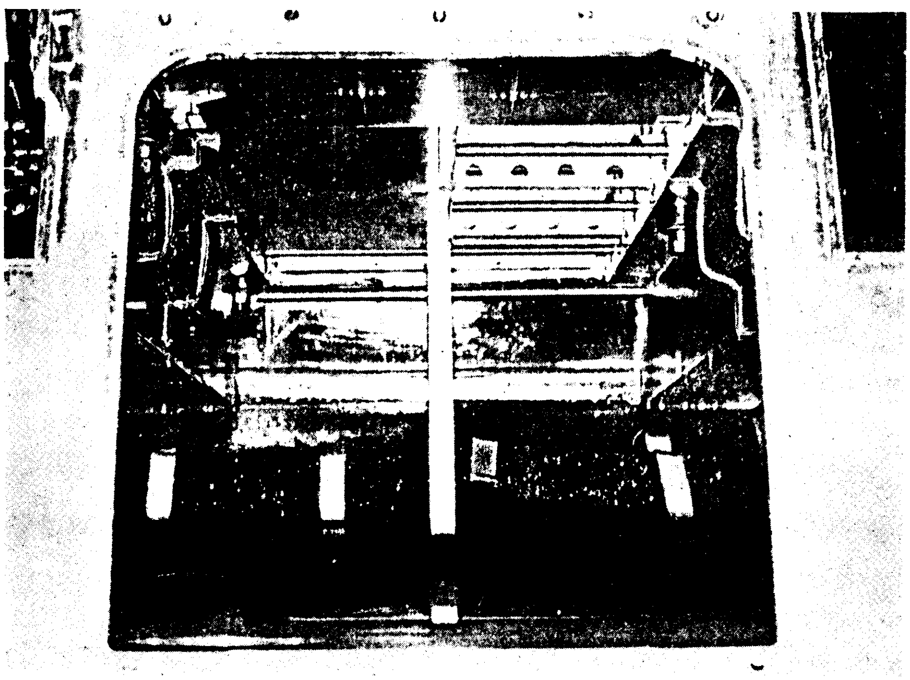

Figure 21. Close-up of 1/6 Scale Model Rear View.

Due to the relative ease with which the cobalt-iron alloy was rolled into foil (see page 22), it was planned to fabricate the plates required for the model from this material. Consequently, a vacuum melted, hot topped, 350 lbs. ingot was obtained from the Special Metals Division of Allegheny Ludlum Corporation. The ingot was 26 inches long and of square cross section, tapered from an eight inch edge to a six inch edge at the bottom. After skinning, the ingot was cut into slabs and hot rolled. Although several plates were obtined, the ingot generally exhibited grain boundary cracking which differed substaintally from the rolling behavior experienced with smaller ingots (i.e. pages 20 thru 22).

Considerable experimentation involving various annealing, hot and warm rolling procedures, etc., were performed in an unsuccessful effort to fabricate high quality, crack-free plates from all portions of the cast cobalt-iron ingot.

Because of the current dollar and time limitations of the project, a back-up set of plates of the high damping iron-chromium-aluminum composition was obtained from the Toshiba Electric Company. The plates were delivered for fabrication in August. Layout, machining and assembly of these plated into the scaled vehicle is presently in progress. It is expected that testing will be completed during November 1976.

A second model evaluation was prepared by casting blades of a torpedo propeller from an alloy of 80^{w}/o Co and 20^{w}/o Fe. Each propeller is composed of an assembly of four blades with an integral hub. A similar assembly is shown in Figure 22.

A single propeller blade made of an aluminum alloy and machined by Bolt, Beranek and Neuman, Inc. was scaled to larger dimension by the application of epoxy compound. The latter procedure was employed to permit fabrication of a casting mold for investment casting which would allow for solidification shrinkage of the cobalt-iron alloy. The mold was made by Hitchiner Manufacturing Company, Inc. Eight propeller blades are being cast using the lost wax method. When these blades have been machined to finished size and inspected, they will be assembled into a propeller which will be tested and evaluated in comparison with existing propellers.

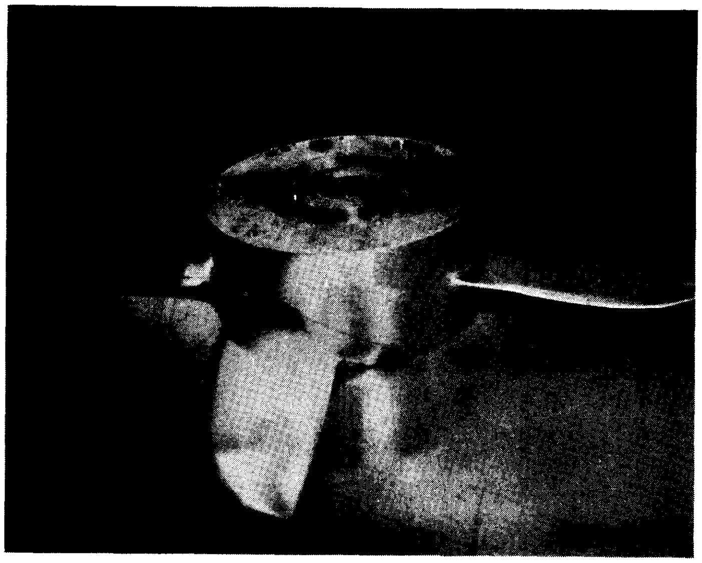

Figure 22. Typical Four Bladed Torpedo Propeller.

V. MECHANISTIC STUDIES OF DAMPING IN ALLOYS.

The ability of a thermoelastic martensite to "store" elastic energy is ultimately connected with the capacity of that same material to continually absorb or damp out vibrational energy. If the mechanism is nonrepeatable, then the damping capacity will deteriorate with the amount of energy absorbed. However, if the energy-absorbing mechanism is repeatable, that is, it is able to return to its original state, then the damping capacity will not readily deteriorate. A martensitic transformation can be used to absorb mechanical vibrations, but if the transformation is nonthermoelastic (such as in the case of most steels), then it is essentially nonrepeatable and much of the strain energy of the transformation is "lost" by the formation of defects in the matrix. The strain energy in a thermoelastic martensitic transformation, however, is stored elastically in the matrix. This elastic strain energy is recoverable, and can aid the reverse transformation. Increasing the thermoelasticity of a martensitic transformation (by increasing the amount of recoverable strain energy in the matrix) improves the cyclability of the transformation and thus promotes the long-term efficiency of energy absorption in the material. The thermodynamic and microstructural studies reported here attempt to provide some insight into the mechanisms of energy absorbtion in Co-Fe and Cu-Al-Ni alloys.

1. Thermodynamics of Thermoelastic Martensitic Transformations

In the last progress report (3) the calorimetry data for Cu-14.0 Al-3.0 Ni were listed. This included data on single crystals, (including single interface and multiple interface transformations), polycrystals, and on nickel plated samples. The calorimetry results from the single interface transformation were shown to directly yield the chemical enthalpy, chemical entropy, and chemical driving force. The results are reviewed in Table 8. Note

TABLE 8

CHEMICAL THERMODYNAMIC QUANTITIES FOR
Cu-14.0Aℓ-3.0Ni CALCULATED FROM CALORIMETRY DATA ON SINGLE
INTERFACE TRANSFORMATIONS

$T_o = 30°C$

$\Delta H_{Chem}^{\beta_1 \to \alpha'} = -123$ cal/mole

$\Delta S_{Chem}^{\beta_1 \to \alpha'} = -0.41$ cal/mole °K

$\Delta G^{\beta_1 \to \alpha'} = -6.5$ cal/mole

---

that there is a change in the T_o (from 42° previously to 30°C), (3) and that this results in a lower chemical driving force of 6.5 cal/mole than the previously reported value of nearly 11 cal/mole. The value of T_o was changed after a re-examination of the calorimetry curves showed an apparently large difference between A_s and A_f. Subsequent examination under a light microscope of the sample which transformed via single interface showed that there was indeed a relatively large difference between A_s and A_f (see Figure 23). This large difference between A_s and A_f is very unexpected in a sample which transformed via single interface. The explanation for this behavior is unclear at the present time; however, it is clear that the reverse transformation (from martensite back to parent) is not by a single interface transformation. The reversion proceeds by a renucleation (of the parent) at several different places in the sample and that these different "plates" (of the parent) in some manner seem to elastically interact with one another during their growth on heating. However, the sample when completely reverted is a single crystal of the parent and upon cooling again undergoes a single interface trans-

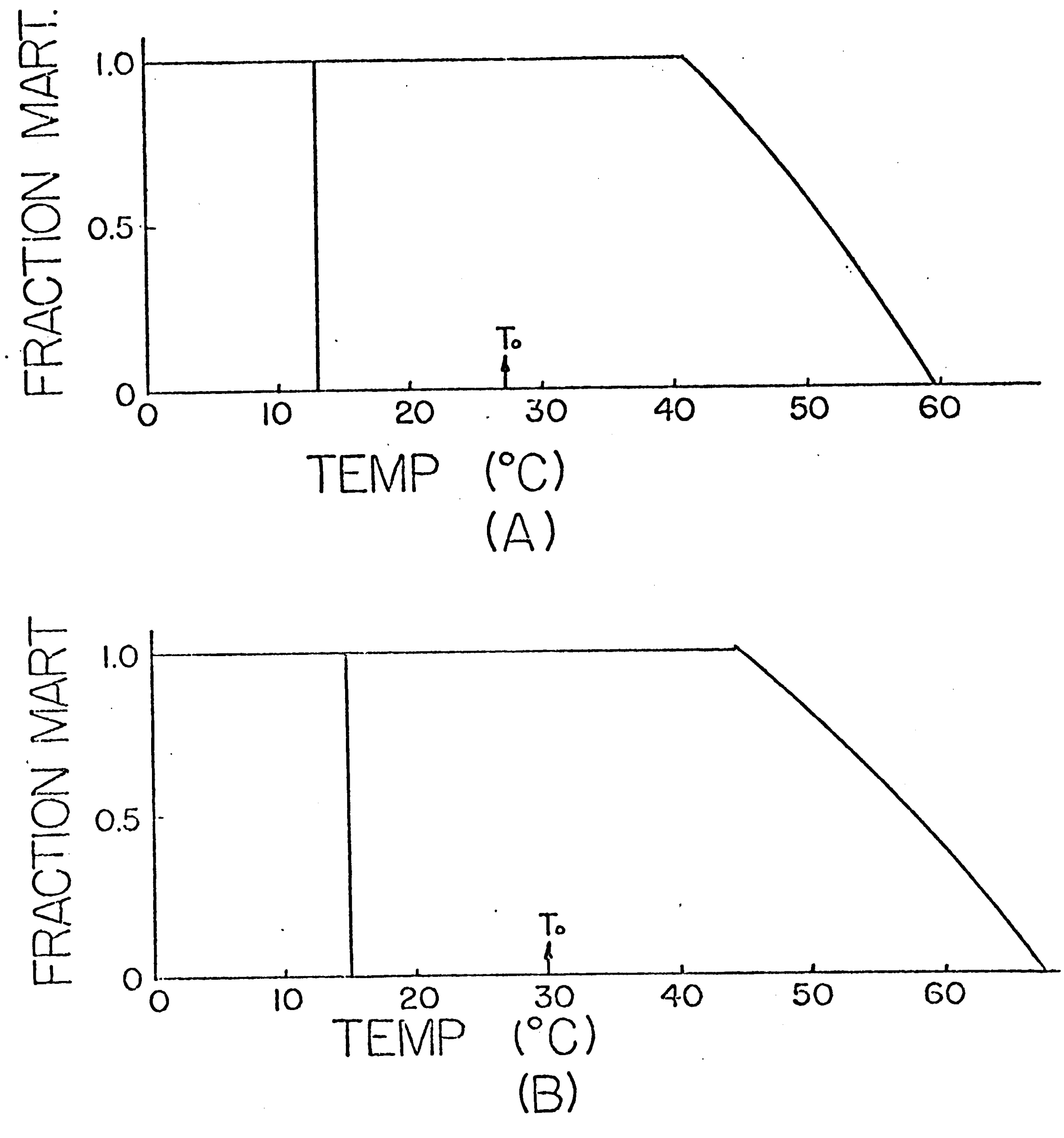

Figure 23. Fraction Martensite Versus Temperature for the Single Interface Transformation of Cu-14.0Al-3.0Ni From (A) Optical Observation and (B) Calorimetry Curves.

formation. The unusual behavior of this sample is not typical of the reverse transformation of Cu-14.0 Al-3.0 Ni--- it is possible that the small sample thickness (i.e. a thin disk) may promote the unusual reversion. Aside from the problem of large difference between A_s and A_f, it is still reasonable to place T_o between M_s and A_s for a single interface transformation. The transformation $\beta_1 \rightarrow \gamma_1$ is nucleated on cooling and progresses to completion without the storage of elastic strain energy (for the single interface transformation) and thus the $\gamma_1' \rightarrow \beta_1$ is nucleated (at A_s) with no effect of elastic stored energy. Assuming that the driving force to nucleate β_1 from γ_1' is approximately the same as the necessary to nucleate γ_1' from β_1 it is then reasonable to place T_o midway between M_s and A_s.

After establishing the chemical thermodynamic terms, it is possible to gain a significant understanding of the effect that elastic strain energy has on the (total) thermodynamic quantities of the transformation. It was evident from the calorimetry results that stored elastic strain energy lowers the measured (i.e., total) enthalpy. Further, the measured enthalpy is decreased as the average transformation temperature is lowered. The average transformation temperature (A.T.T.) here is used to denote the temperature at which a large amount of the sample (on the order of 50%) has transformed. The A.T.T. and also the measured enthalpy are lowered when the samples are transformed by a multiple plate sequence - this allows an increase in the amount of the transformational shape change stored as strain energy. The amount of the shape change stored as strain energy determines the thermoelasticity of the transformation, and it has been shown (in the last progress report) that the amount of stored strain energy can be controlled (at least coarsely). Specifically, such things as sample preparation, grain size, and nickel plating have been shown to affect the

thermoelasticity of the transformation. Nickel plating or fine grain size for example, cause the transformation to proceed as a finer multiple interface sequence than in a typical single crystal, and this causes the effect of strain energy to become larger.

The basic concept of thermoelasticity involves a balance between elastic and chemical free energies. However, when the interface between the parent and the martensite is in motion, a "frictional stress" for interfacial motion should be included. This frictional stress can be approximated by considering the irreversible work done when a shear stres τ_o is required to move an interface which accomplishes the transformation strain γ_T. The force balance on the interface then becomes

$$\Delta G_{chem} + n\Delta G_{elas} = \pm \tau_o \gamma_T \tag{1}$$

where the frictional term is positive during heating (i.e. the reverse transformation) and negative during cooling (i.e. the forward transformation). ΔG_{chem} is the chemical free energy change for the β_1 to γ_1' transformation, ΔG_{elas} is the change in free energy due to the contributions of stored elastic strain energy, and n is a constant.

In the case of a single interface transformation, the effects of elastic strain energy are eliminated and, to a good approximation, the entire hysteresis involved in moving an existing parent-martensite (P-M) interface is caused by the existence of a frictional resistance to the motion of that interface. That is, a sufficient chemical driving force must be built up (by cooling below T_o for the forward transformation or heating above T_o for the reverse transformation to overcome the "resistance" of the frictional stress. The fricitional term can be estimated by measuring the chemical driving force necessary to move an existing P-M interface by finding the undercooling (below T_o) and

the superheating (above T_o) necessary to drive the interface in opposite directions. For a single interface transformation, Equation (1) becomes:

$$\Delta G_{chem} = -T_o \gamma_T \tag{2}$$

and further ΔG_{chem} can be found if the chemical entropy and T_o are known, along with T_g (the temperature at which the interface grows in the forward or reverse directions).

$$\Delta G_{chem_{T_g}} = -T_o \gamma_T = \Delta S(T_o - T_g) \tag{3}$$

The frictional term arrived at by measurement of the hysteresis involved in moving the interface (in the single interface transformation) in opposite directions is about ±5.7 cal/mole. Figure 24 shows how the absolute value of $\Delta H_{measured}$ is decreased as the average temperature of the transformation is lowered. The experimental points are the measured (total) enthalpies for the Cu-14.0 Al-3.0 Ni single crystal chips which were cut from the same initial (large) single crystal sample. The measured enthalpies of the same single crystal chips which were nickel plated are also included in Figure 24. The chemical enthalpy was found to be -123 cal/mole (previously described), and because the temperature hysteresis caused by the frictional term is present in every transformation, whether single interface or not, this suggest that ΔH_{chem} should be placed below T_o. The amount that ΔH_{chem} is placed below T_o is approximately determined from the measurements of the hysteresis involved in moving the P-M interface back and forth during a single interface transformation.

In Figure 24, ΔH_{chem} is placed at T_g (=289°K) which is about 14°K below T_o. The data were fit with a least squares straight line which was forced to go through ΔH_{chem} at 289°K.

The straight line through the data was selected because it provides a reasonable fit, and this then provides a functional dependence of ΔH_{net}, and thus ΔH_{elas} (where $\Delta H_{elas} = \Delta H_{net} - \Delta H_{chem}$) on temperature. It is emphasized that the straight line fit is an assumption used as a convenient starting point; there is no apriori reason to expect a linear dependence of ΔH_{net} on temperature.

Elastic entropy is often considered to be a negligibly small quantity, and when this is true, it follows that

$$\Delta G_{elas} = \Delta H_{elas} \tag{4}$$

For the system being studied here, ΔH_{chem} is known to be equal to -123 cal/mole. Further, the approximate temperature dependence of ΔH_{net} is known form Figure 24, and thus ΔH_{elas} can be found from the following relationship:

$$\Delta H_{elas} = \Delta H_{net} - \Delta H_{chem} \tag{5}$$

In the previous reports, where the chemical thermodynamic terms were found, it was shown that

$$\Delta G_{chem}(T) = \Delta S_{chem}(T_o - T) \tag{6}$$

and from Table 8 we seen that ΔS_{chem} equals -0.41 cal/mole °K and T_o equals 30°C. Referring again to Equation 1 and realizing that the frictional term is constant, it is readily apparent that a plot of $(\Delta G_{chem} + T_o\gamma_T)$ versus $\Delta H_{elastic}$ (which is assumed to approximately equal ΔG_{elas}) should yield a value of n. This plot is shown in Figure 25, and the slope is found to be equal to -0.27, indicating that n has a value of 0.27. A value of n less than 1.0 physically means that more energy was stored elas-

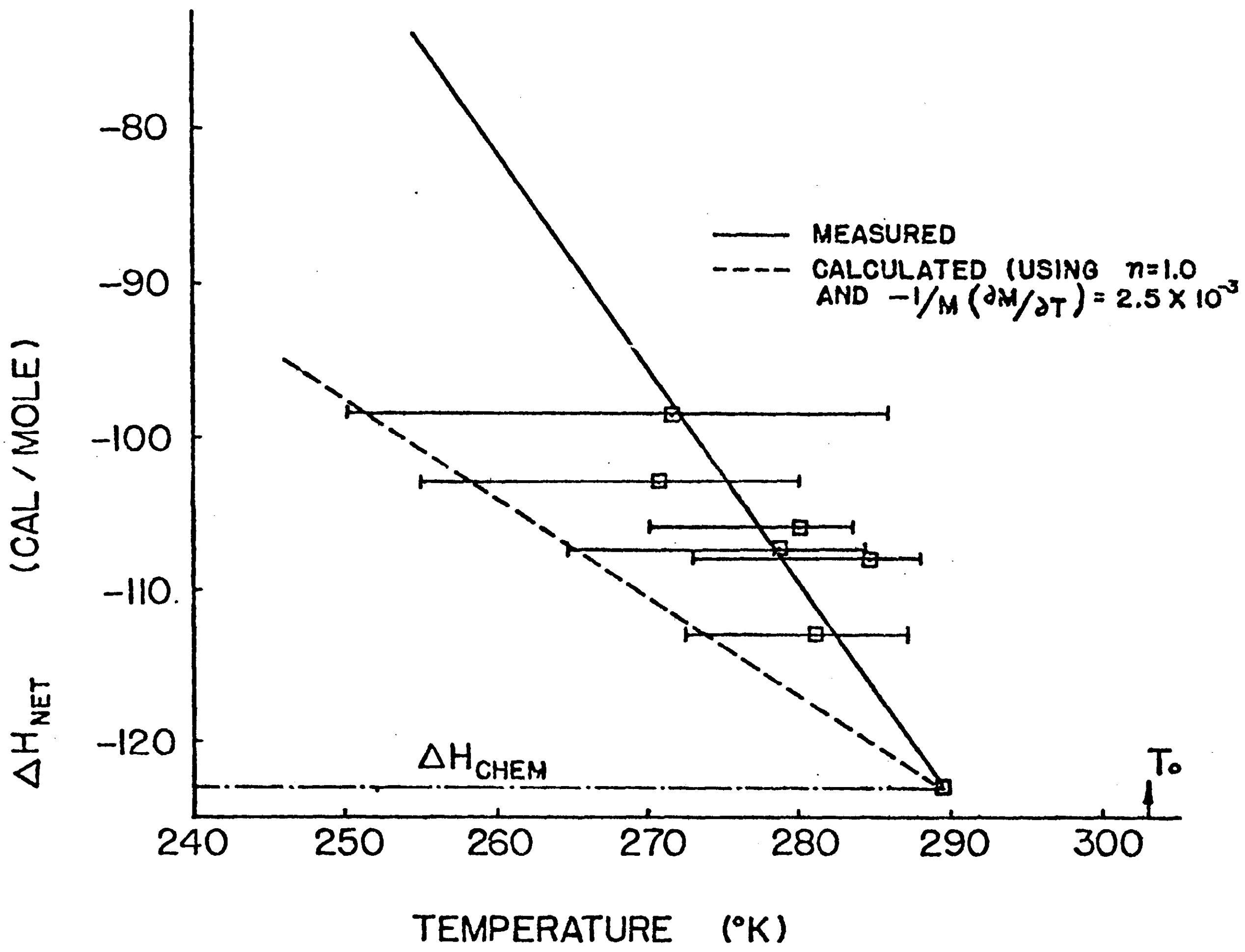

Figure 24. Change in the Net Enthalpy Versus Temperature for Single Crystals of Cu-14Al-3Ni.

tically than was available from the chemical free energy change (i.e. a violation of the First Law of Thermodynamics). Since n was found to be a number less than 1.0, this demonstrates that it is a poor assumption to use the approximation that $\Delta G_{elas} = \Delta H_{elas}$. Specifically, contributions from changes in elastic entropy to the elastic free energy change are not negligible for the case of $\beta_1 \rightarrow \gamma_1'$ transformation in Cu-14Al-3Ni.

In order to arrive at the approximate contribution of elastic entropy to the elastic free energy change, the elastic entropy change (as a function of temperature) was related to the change of some appropriate modulus as a function of temperature. The specific relationship is:

$$\frac{\Delta S_{elas}}{\Delta G_{elas}} = \frac{-1}{M} \frac{dM}{dT} \qquad (7)$$

where M is some particular modulus (which depends on the shape change of the transformation). Data for Young's Modulus (19) and for the shear modulus (20) show that $\frac{-1}{M} \frac{dM}{dT}$ to be of the order of 2×10^{-3} to $3 \times 10^{-3}/°K$ for Cu-Al-Ni specimens which undergo the $\beta_1 \rightarrow \gamma_1$ transformation on cooling. Using a value of $\frac{-1}{M} \frac{dM}{dT}$ equal to $2.5 \times 10^{-3}/°K$, ΔS_{elas} can be calculated as a function of temperature, (using n=1). After having ΔS_{elas} as a function of temperature, ΔH_{elas} can be calculated by using:

$$\Delta H_{elas} = \Delta G_{elas} + T\Delta S_{elas} \qquad (8)$$

and thus ΔH_{net} as a function of temperature can be obtained by substitution into Equation 5. This calculated value of ΔH_{net} as a function of temperature is also shown (as a dashed line) in Figure 24. It is apparent that there is still a rather large discrepancy between the measured data points and the line calculated by using values of the temperature dependence of the modulus and an assumed value of n (the upper limit value of 1.0

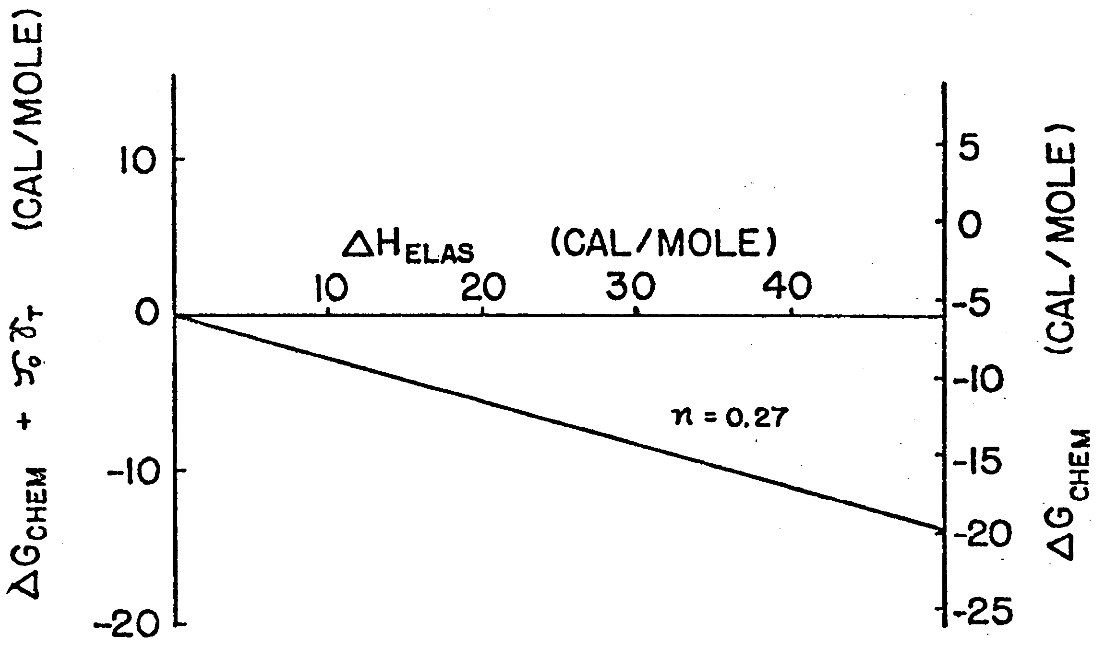

Figure 25. Change in Chemical Free Energy Plus Frictional Term Versus the Change in Elastic Enthalpy as Calculated from Calorimetry Data of Cu-14Al-3Ni.

was used). The width of the calorimeter peak is included for each point, and it is obvious that the calculated line fits the lower limits of the peaks much better than it fits the average transformation temperatures. It is, in fact, reasonable to assert that forcing the fit through the average transformation temperature is really an upper limit for the functional dependence of ΔH_{net} on temperature. This is because most of the elastic energy (specifically in the data from single crystal samples reported in Figure 24) is stored in the sample as the multiple interface transformation approaches completion. As the transformation proceeds, the martensite plates impinge upon, and constrain each other, and this impingement and constraint become highest (i.e. more strain energy is stored per unit volume) near the end of the transformation. The actual temperature dependence of ΔH_{net} should then probably be biased more toward the lower end of the transformation peak than to the center of mass (i.e. A.T.T.) of the peak. This may account for a portion of the difference between the experimental and calculated lines, however, it certainly cannot be the cause of the entire difference between the two.

The remaining difference between the experimental line and the line calculated from modulus data could possibly be due to a significant increase in the amount of interfacial area due to twins (and/or stacking faults) as the martensite plates become finer and finer. In the present work it has been found that the number of martensite plates increase and correspondingly the plate size decreases as the A.T.T. is lowered. It has further been reported in the Cu-Al system (which under goes the same transformation from β_1 to γ_1') that the twin spacing decreases with the size of the martensite plate (21). In alloys of Cu-Al-Ni which undergo the $\beta_1 \rightarrow \gamma_1'$ transformation, it has also been reported that the width of twins varies significantly

from one plate to another; however, no correlation was made with overall plate size (22).

The contribution of twin boundaries to the net change in enthalpy (ΔH_{TB}) is given approximately by:

$$\Delta H_{TB} = \gamma V_m \frac{1}{d} \tag{9}$$

where γ is the boundary interfacial energy (= 30 ergs/cm^2), V is the molar volume (= 7.46 cm^3/mole), and d is the twin spacing. In order for the increase in twin boundary area (or stacking fault area) to account for the discrepancy in Figure 24 (of about 10 cal/mole at 275°K) the spacing between twins (or faults) would have to be on the order of 50 Å. On the other hand, the interface spacing (twin and/or stacking fault) would have to be above about 500 Å in the single interface sample (i.e. the sample which transformed at 289°K) in order that the contribution to the enthalpy change from interface energy be negligible. The information available on the microstructure of Cu-Al-Ni shows that the twin spacing in large martensite plates can be on the order of 500 to 1000 Å. It is also apparent that stacking faults can form with a fine spacing in some martensite plates, but this unfortunately cannot be correlated with the size of the martensite plates. Further experimental observations on replicas and thin foils of γ' martensites in Cu-Al-Ni are needed to substantiate whether changes in twin or fault density are sufficient to explain the difference between the experimental and calculated lines in Figure 24.

2. Mechanisms of Damping in Co-Fe and Cu-Al-Ni Alloys

A. Co-Fe Alloy

A major goal of the present research program is to identify the damping causing mechanism(s) in potential structural materials which exhibit high damping capacities. The mechanisms

suspected of causing the major portion of the damping in the materials identified in this program as having the highest damping capacities are of the static hysteresis type. The specific type of mechanism is thought to involve the motion of twin boundaries, stacking faults, magnetic domain boundaries and the interfaces between parent and martensitic phases. Damping caused by the motion of interfaces is usually characterized by being amplitude dependent, as well as being essentially frequency independent. That is, the damping depends on the maximum stress applied to the sample during testing, but not on the frequency. The amplitude dependence of the Co-Fe alloy, which is considered to be a main candidate material, has been shown in prior reports. The frequency dependence of the high damping Co-Fe alloys has not yet been measured.

It has been described in previous reports (2-3) how the Co-Fe alloys with a composition near 80 w/o Co - 20 w/o Fe are close to undergoing a fcc-bcc transformation at room temperature. Also the 80Co-20Fe alloy has a Curie temperature which is quite high -- near 950°C. The experimentally determined damping in various Co-Fe alloys (with compositions near 80Co-20Fe) shows a very strong dependence on whether the alloy is completely fcc (high damping) or is bcc or some mixture of fcc and bcc (lower damping). Since the Curie temperature in both the fcc and bcc phases is very high, it was thought that magnetic domain wall motion damping was the cause of only a portion of the total damping. It has been shown in the damping tests that the damping of a suitably heat treated 80Co-20Fe sample was reduced by approximately 55% when a saturating magnetic field was applied during testing. This indicates that although magnetic domain wall damping is important, it is not the sole damping causing mechanism. Because the 80Co-20Fe alloy exhi-

bits the highest damping when the alloy is all fcc (and seemingly about to transform to bcc) it was proposed that much of the damping is caused by the alloy being in a metastable phase condition. The exact nature of the mechanism causing the high damping was, however, not specified. With the intention of identifying possible damping causing mechanisms, a study of the microstructure was initiated. In past reports, (2-3), optical micrographs of the 80Co-20Fe alloy in various conditions were shown, including micrographs displaying the magnetic domain structure (3). In the present report, a preliminary set of electron micrographs are shown in Figures 26 and 27.

The 80Co-20Fe alloy was rolled (with intermediate anneals at 1000°C) to a sheet of approximately 1.5 mils thickness, then annealed at 1150°C (in a quartz capsule backfilled with argon) for two hours. Samples were then either air cooled (in the unbroken capsule) or water quenched (with the capsule broken). Electron transparent foils were then obtained by electropolishing the thin annealed sheet in a solution of 80 methanol-20 perchloric acid (at -40°C and about 15 volts). The polish of the heat-treated sheet was very uneven -- thinnest portions of the sample showed that they were uniformly perforated with a large number of fine holes. The samples behaved as though they were composed of a two-phase mixture with one-phase preferentially electrolytically attacked.

A T.E.M. micrograph of the air-cooled sample is shown in Figure 26. The matrix was essentially devoid of major faults, including stacking faults, dislocation arrays, etc. The thin area had an overall mottled appearance. The cause of this appearance may be caused by a fine two-phase mixture, but the diffraction patterns were of insufficient quality to confirm this. The diffraction patterns did, however, show the matrix to be fcc. It is also of interest to note that,

Figure 26. Transmission Electron Micrograph of Air Cooled 80Co-20Fe (Magnification 45000X)

using the Lorentz technique for imaging ferromagnetic domains, the samples failed to show any magnetic domain structure.

Figure 27 shows T.E.M. micrographs of a sample of 80Co-20Fe which was water quenched. The general appearance of most of the thin area is shown in Figure 27a -- that is, it is a coarsely mottled structure. This again may be due to a coherent two-phase structure, but the diffraction patterns were not of a high enough quality to support this. The matrix was indexed as fcc. Underfocussing of the image shown in Figure 27a yields the micrograph shown in Figure 27b which displays the magnetic domain structure of the sample. Figure 27c shows some straight lined faults which were observed in some of the thin area of the water-quenched sample -- they give the appearance of being stacking faults, but in this preliminary examination these faults were not fully identified.

The primary results of the initial look at the microstructures of air cooled (in capsule), and water quenched 80Co-20Fe are that [1] the air-cooled samples examined exhibited no major faults or interfaces, including no magnetic domain structure, and [2] the water-quenched sample on the other hand did show some major faults and also exhibited a magnetic domain strucuture.

B. Cu-Al-Ni Alloy

Previous reports as well as articles in the literature have identified Cu-14Al-3Ni (which undergoes the $\beta_1 \to \gamma_1'$ transformation) as a high damping material. The mechanisms postulated as being the cause of the high damping have included the motion of the parent-martensite (P-M) interface, martensite-martensite (M-M) interfaces, and twin boundaries. Electron microscopy work by Otsuka (<u>23</u>) has demonstrated the ability of twins to move as

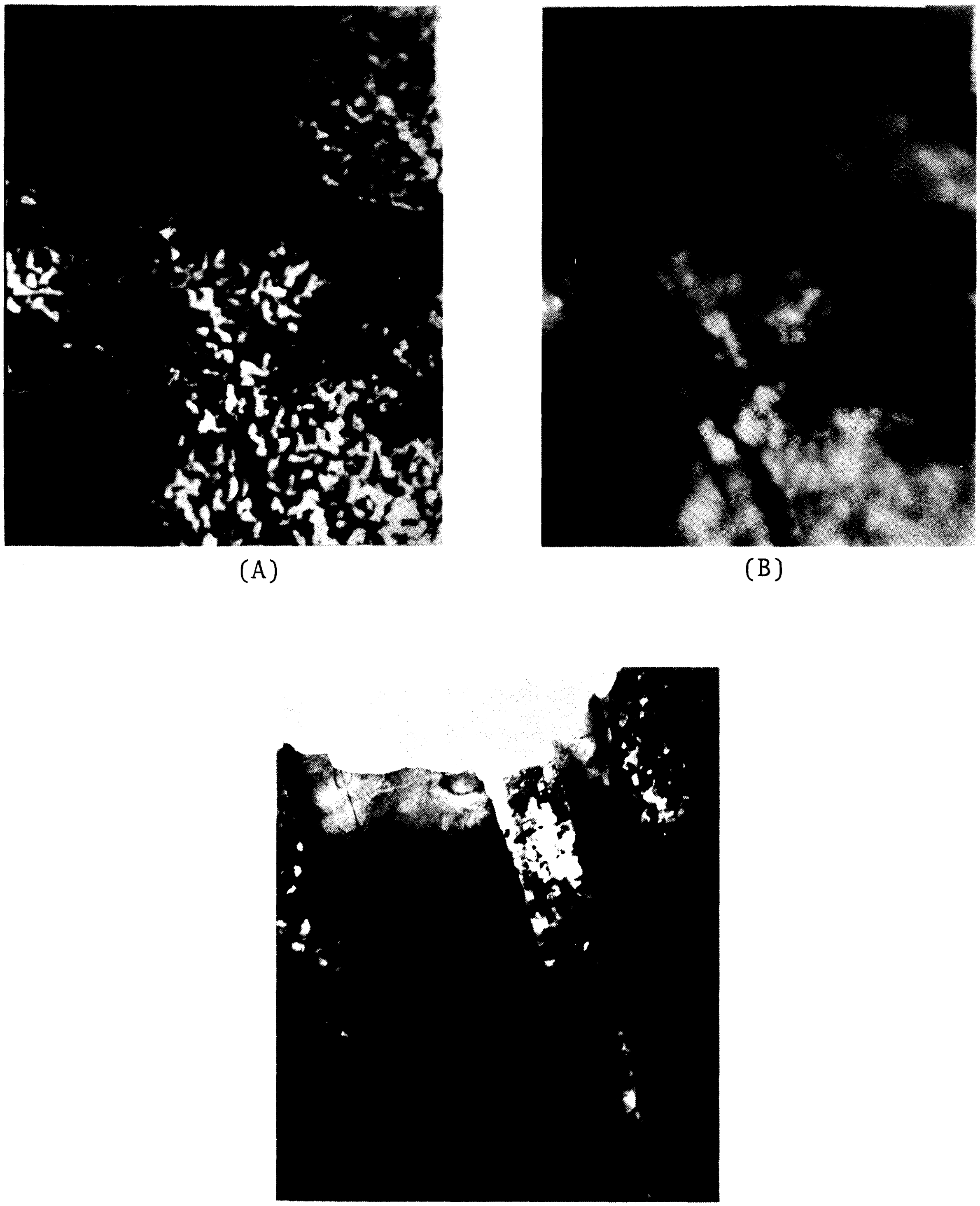

(A)

(B)

(C)

Figure 27. Transmission Electron Micrographs of Water Quenched 80Co-20Fe (Magnification 45000X) (a) General Matrix Appearance, (b) Underfocussed Image Showing Magnetic Domain Structure, and (c) Straight Lined Faults in the Matrix.

an external stress is applied to the sample. There is thus microstructural evidence that twin boundaries are glissile and therefore by their stress-induced motion can cause static hysteresis type damping (24).

The optical micrographs shown in Figure 28 and 29 show that P-M interfaces can also move forward with stress and revert with no time delay. Tensile stresses on the order of 5000 psi were applied to samples being held at constant temperature. In Figure 28 the sample was at a temperature of 40°C which is about 35°C above M_s. Figure 28a is the microstructure with no stress applied,* and in Figure 28b a stress (of approximately 5000 psi) was applied. (Note that the number and width of the acicular martensite has increased). In Figure 28c the stress was again returned to zero, and the microstructure has been reverted to very close to the first microstructure shown in 28a. The acicular martensite formed by stressing the matrix well above M_s has been identified by Otsuka and Shimizu (25) as being of the β_1'(or 9R) type compared to the thermally formed γ_1' (or 2H) type.

As the temperature is moved closed to M_s, the stress-induced martensite is the same as the thermally formed (or γ_1' 2H). Figure 29a shows the Cu-14Al-3Ni sample just below M_s; the thermally formed martensite is platelike and is shown by the arrows in the micrograph. In Figure 29b with a stress applied (again roughly 5000 psi), existing plates have increased in both thickness and length (see arrows) and new plates of γ_1' have been formed. As in the previous example, when the stress

---

* Earlier in the sample's history, however, stress had been applied which induced the non-reverted acicular-type martensite seen in the micrograph.

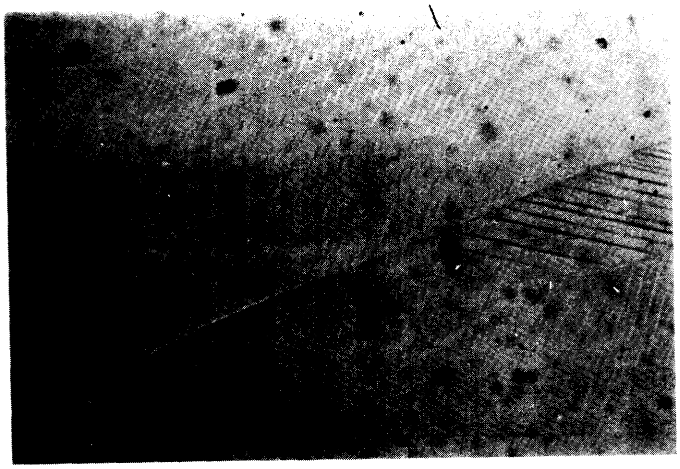

(A)

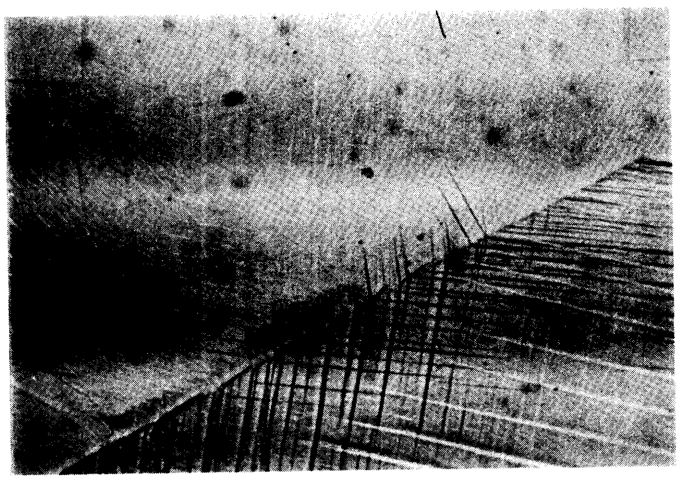

(B)

(C)

Figure 28. Optical Micrograph (Magnification 50X) of Cu-14Al-3Ni At a Temperature 36°C above M_S. (a) Unstressed, (b) Applied Stress of 5000 psi, and (c) Stress Released.

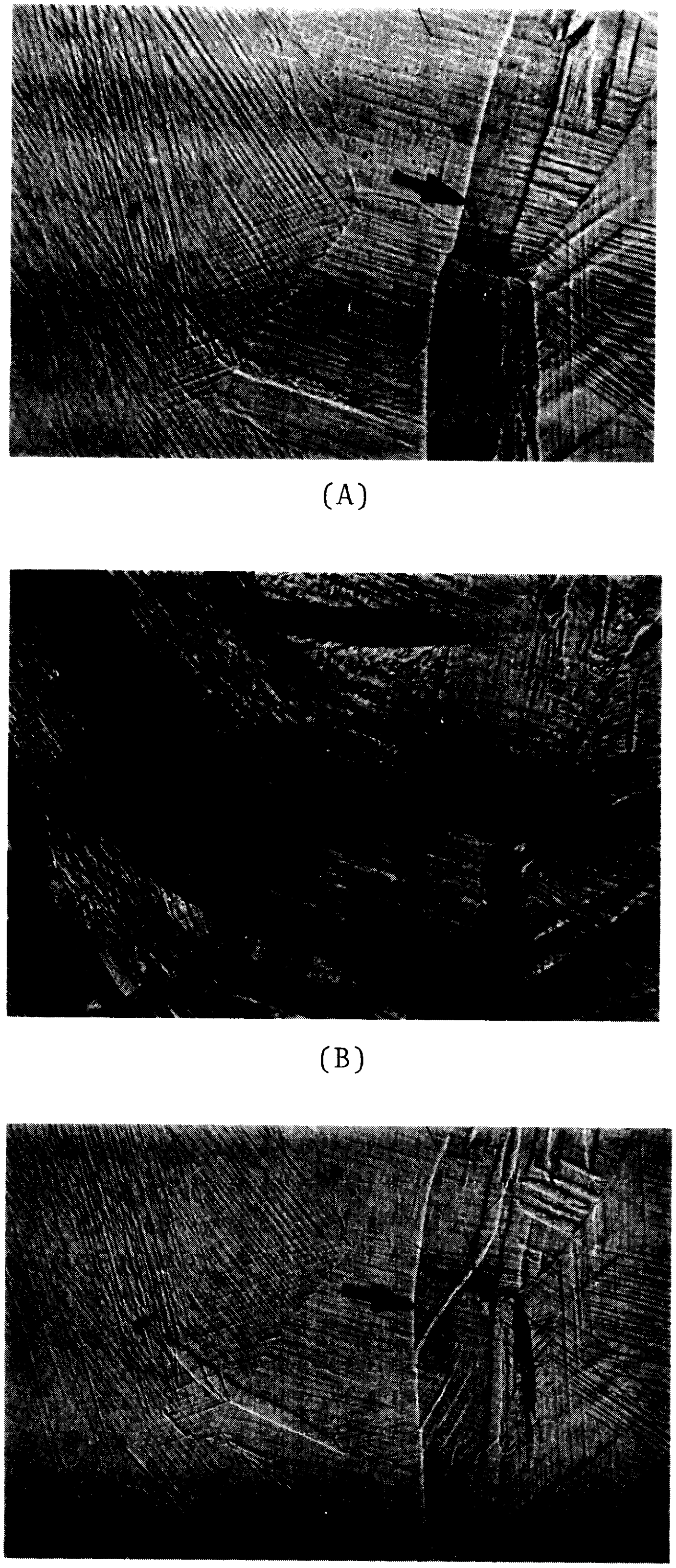

(A)

(B)

(C)

Figure 29. Optical Micrograph (Magnification 50X) of Cu-14Al-3Ni at a Temperature Just Below M_s. (a) Unstressed, (b) Applied Stress of 5000 psi, and (c) Stress Released.

is released (Figure 29c), the microstructure returns close to what it was in the unstressed state (in Figure 29a).

The results of these two experiments show that for stresses on the order of those employed in testing the damping of the samples (2 → 5000 psi), that P-M interfaces can indeed move. Further, they are glissile in both directions and are not necessarily prevented from returning to their original position when the stress is released (or the sample is stressed in the opposite sense). As with twin boundaries, the motion of P-M interfaces requires a certain amount of force and energy may be dissipated during the boundary motion, thus providing a damping mechanism.

Work will continue in order to examine whether or not M-M interfaces can move under (fairly small) stresses and therefore exist as a third possible damping mechanism in thermoelastic martensites.

REFERENCES

1. L. Kaufman, S. A. Kulin and P. P. Neshe, "Noise Abatement and Internal Vibrational Absorption in Potential Structural Materials," AMMRC CTR 75-4, Contract DAAG46-74-C-0048, ARPA Order 2555, March 1975, ManLabs, Inc., Cambridge, Massachusetts 02139.

2. L. Kaufman, S. A. Kulin and P. P. Neshe, "Noise Abatement and Internal Vibrational Absorption in Potential Structural Materials," AMMRC CTR 75-4, Contract DAAG46-74-C-0048, ARPA Order 2555, Sept. 1975, ManLabs, Inc., Cambridge, Massachusetts 02139.

3. L. Kaufman, S. A. Kulin and P. P. Neshe, "Noise Abatement and Internal Vibrational Absorption in Potential Structural Materials," AMMRC CTR 75-4, Contract DAAG46-74-C-0048, ARPA Order 2555, March 1976, ManLabs, Inc., Cambridge, Massachusetts 02139.

4. A. Cochardt, Magnetic Properties of Metals and Alloys, A.S.M., Cleveland (1959) 251-279., Tr. A.I.M.E. (1956) 206 1295.

5. J. C. Fister and S. Shapiro, "Improved High Damping Copper-Base Alloys," International Copper Research Association Project 221, Final Report, September 1974, Olin Metals Research Laboratories, New Haven, Connecticut 06504.

6. J. Perkins, G. R. Edwards and N. Hills, "Materials Approaches to Ship Silencing," June 1974, NPS-59Ps74061, Naval Post Graduate School, Monterey, California.

7. J. F. Nachman, J. C. Napier and A. N. Hammer, "Development of Cu-Mn Base Alloys with High Damping Properties," Internatioanal Copper Research Association Report No. 152, Final Report March 1970, Solar Division, International Harvester Corporation, San Diego, California 92112.

8. J. F. Nachman, J. C. Napier and A. N. Hammer, "Development of Cu-Mn Base Alloys with High Damping Properties," International Copper Research Association Project No. 152A, Final Report, March 1971, Solar Division, International Harvester Corporation, San Diego, California 92112.

9. L. Kaufman and H. Nesor, Zeit. Metallkunde (1973) 74 249.

10. K. C. Mills, M. J. Richardson and P. J. Spencer, "Thermodynamic Properties and Phase Diagram of the Fe-Co and Ni-Pt Systems," Faraday Soc. Symposium (In Press).

11. H. Schumann, "Cobalt," (1968) 40 156.

12. U. Hashimoto, J. Japanese Inst. of Metals (1937) 1 177.

13. K. Ishida and T. Nishizawa, Tr. Jap. Inst. of Metals (1974) 15 225.

14. L. Kaufman, Metallurgical Transactions (1969) 245 91.

15. J. M. Vitek and H. Warlimont (1975) (Submitted for publication in Metal Science).

16. Y. Z. Vintaykin, D. F. Litvin and V. A. Udorenko, Fiz. Metal, Metall., 37 No. 6, 1974, 1228.

17. Toshiba Electric Co., R and D Center, Kawasaki City, Kanagawa, 210 Japan.

18. T. R. Norris "Tracked Vehicles: Model Study on the Effect of Track Parameter Changes on the Acoustic Signature, Seismic Signature and Interior Noise" Bolt, Beranek and Newman Inc., Report No. 3031, submitted to U. S. Army Tank-Automotive Command, Warren Michigan (1975), (Contract DAAE07-74-C-0002).

19. Sugimoto El Al., Scripta Met. 8 (1974) 1341.

20. Teplov Etal., Fiz. Metal. Metalloved 27, No. 2 (1969) 339.

21. Greninger, A., Tr. A.I.M.E. (1939) 133 204.

22. Otsuka, K. and K. Shimizu, Tr., J.I.M. (1974) 15 109.

23. Otsuka, K., J. of Applied Phys. (1971) 10 571.

24. Zener, C., Elasticity and Anelasticity of Metals, University of Chicago Piess, Chicago, Illinois (1948).

25. Otsuka, K., and K. Shimuzu, Phil. Mag., (1971 24 481.

DISTRIBUTION LIST

No. of Copies	To
1	Office of the Director, Defense Research and Engineering, The Pentagon, Washington, D. C. 20301
12	Commander, Defense Documentation Center, Cameron Station, Building 5, 5010 Duke Street, Alexandria, Virginia 22314
1	Metals and Ceramics Information Center, Battelle Columbus Laboratories, 505 King Avenue, Columbus, Ohio 43201
	Chief of Research and Development, Department of the Army, Washington, D. C. 20310
2	ATTN: Physical and Engineering Sciences Division
	Commander, Army Research Office, P. O. Box 12211, Research Triangle Park, North Carolina 27709
1	ATTN: Information Processing Office
	Commander, U. S. Army Materiel Development and Readiness Command, 5001 Eisenhower Avenue, Alexandria, Virginia 22333
1	ATTN: DRCDE-TC
	Commander, U. S. Army Electronics Command, Fort Monmouth, New Jersey 07703
1	ATTN: DRSEL-GG-DD
1	DRSEL-GG-DM
	Commander, U. S. Army Missile Command, Redstone Arsenal, Alabama 35809
1	ATTN: Technical Library
1	DRSMI-RSM, Mr. E. J. Wheelahan
	Commander, U. S. Army Armament Command, Rock Island, Illinois 61201
2	ATTN: Technical Library
1	DRSAR-SC, Dr. C. M. Hudson
1	DRSAR-PPW-PB, Mr. Francis X. Walter
	Commander, U. S. Army Satellite Communications Agency, Fort Monmouth, New Jersey 07703
1	ATTN: Technical Document Center
	Commander, U. S. Army Tank-Automotive Research and Development Command, Warren, Michigan 48090
2	ATTN: DRDTA, Research Library Branch
	Commander, White Sands Missile Range, New Mexico 88002
1	ATTN: STEWS-WS-VT
	Commander, Aberdeen Proving Ground, Maryland 21005
1	ATTN: STEAP-TL, Bldg. 305

No. of Copies	To
	Commander, Frankford Arsenal, Philadelphia, Pennsylvania 19137
1	ATTN: Library, H1300, Bl. 51-2
1	SARFA-L300, Mr. J. Corrie
	Commander, Picatinny Arsenal, Dover, New Jersey 07801
1	ATTN: SARPA-RT-S
	Commander, Redstone Scientific Information Center, U. S. Army Missile Command, Redstone Arsenal, Alabama 35809
4	ATTN: DRSMI-RBLD, Document Section
	Commander, Watervliet Arsenal, Watervliet, New York 12189
1	ATTN: SARWV-RDT, Technical Information Services Office
	Commander, U. S. Army Foreign Science and Technology Center, 220 7th Street, N. E., Charlottesville, Virginia 22901
1	ATTN: DRXST-SD2
	Director, Eustis Directorate, U. S. Army Air Mobility Research and Development Laboratory, Fort Eustis, Virginia 23604
1	ATTN: Mr. J. Robinson, SAVDL-EU-SS
	Librarian, U. S. Army Aviation School Library, Fort Rucker, Alabama 36360
1	ATTN: Building 5907
	Naval Research Laboratory, Washington, D. C. 20375
1	ATTN: Dr. J. M. Krafft - Code 8430
	Chief of Naval Research, Arlington, Virginia 22217
1	ATTN: Code 471
	Air Force Materials Laboratory, Wright-Patterson Air Force Base, Ohio 45433
2	ATTN: AFML/MXE/E. Morrissey
1	AFML/LC
1	AFML/LLP/D. M. Forney, Jr.
1	AFML/MBC/Mr. Stanley Schulman
	National Aeronautics and Space Administration, Washington, D. C. 20546
1	ATTN: Mr. B. G. Achhammer
1	Mr. G. C. Deutsch - Code RR-1
	National Aeronautics and Space Administration, Marshall Space Flight Center, Huntsville, Alabama 35812
1	ATTN: R-P&VE-M, R. J. Schwinghamer
1	S&E-ME-MM, Mr. W. A. Wilson, Building 4720
	Wyman-Gordon Company, Worcester, Massachusetts 01601
1	ATTN: Technical Library

DISTRIBUTION LIST

No. of Copies	To
1	Office of the Director, Defense Research and Engineering, The Pentagon, Washington, D. C. 20301
12	Commander, Defense Documentation Center, Cameron Station, Building 5, 5010 Duke Street, Alexandria, Virginia 22314
1	Metals and Ceramics Information Center, Battelle Columbus Laboratories, 505 King Avenue, Columbus, Ohio 43201
	Chief of Research and Development, Department of the Army, Washington, D. C. 20310
2	ATTN: Physical and Engineering Sciences Division
	Commander, Army Research Office, P. O. Box 12211, Research Triangle Park, North Carolina 27709
1	ATTN: Information Processing Office
	Commander, U. S. Army Materiel Development and Readiness Command, 5001 Eisenhower Avenue, Alexandria, Virginia 22333
1	ATTN: DRCDE-TC
	Commander, U. S. Army Electronics Command, Fort Monmouth, New Jersey 07703
1	ATTN: DRSEL-GG-DD
1	DRSEL-GG-DM
	Commander, U. S. Army Missile Command, Redstone Arsenal, Alabama 35809
1	ATTN: Technical Library
1	DRSMI-RSM, Mr. E. J. Wheelahan
	Commander, U. S. Army Armament Command, Rock Island, Illinois 61201
2	ATTN: Technical Library
1	DRSAR-SC, Dr. C. M. Hudson
1	DRSAR-PPW-PB, Mr. Francis X. Walter
	Commander, U. S. Army Satellite Communications Agency, Fort Monmouth, New Jersey 07703
1	ATTN: Technical Document Center
	Commander, U. S. Army Tank-Automotive Research and Development Command, Warren, Michigan 48090
2	ATTN: DRDTA, Research Library Branch
	Commander, White Sands Missile Range, New Mexico 88002
1	ATTN: STEWS-WS-VT
	Commander, Aberdeen Proving Ground, Maryland 21005
1	ATTN: STEAP-TL, Bldg. 305

No. of Copies	To
1	A. V. Illyn, Technical Director, Babcock & Wilcox, Old Savannah Road, Augusta, Georgia 30903
1	Mr. W. J. Welsch (Code 224), Naval Materials Industry Resources Office, N.A.E.C., Building #537, Philadelphia, Pennsylvania 19112
1	Mr. R. E. Cross, Federal Die Casting Co., 2222 Elston Avenue, Chicago, Illinois 60614
1	Captain Ebenezer F. Porter, 2618 S. Lynn Street, Arlington, Virginia 22202
1	Mr. Charles E. Bates, Head, Metallurgy Section, Southern Research Institute, 2000 Ninth Avenue, South, Birmingham, Alabama 35205
1	Mr. R. F. Kirby, Chief, Materials Engineering Dept., Dept. 93-39M, Airesearch Manufacturing Company of Arizona, 402 South 36th Street, P. O. Box 5217, Phoenix, Arizona 85010
1	Dr. Mervin T. Rowley, American Foundry Men's Society, Golf & Wolf Roads, Des Plaines, Illinois 60016
1	William R. Freeman, Jr., Howmet Corporation, Vice President and Technical Director, Technical Center, Gas Turbine Components Group, 699 Benston Road, Whitehall, Michigan 49461
1	Dole A. Marek, General Motors Corporation, Detroit Diesel Allison, 4700 W 10th Street, Indianapolis, Indiana 46206
	General Dynamics, Convair Aerospace Division, P. O. Box 748, Ft. Worth, Texas 76101
1	ATTN: Mfg. Engineering Technical Library
1	Dr. Robert Mehrabian, Dept. of Metallurgy & Mining Engineering, University of Illinois, Urbana, Illinois 61801
1	Robert McNally, Research Library, Special Metals Corporation, Middle Settlement Road, New Hartford, New York 13413
	Director, Army Materials and Mechanics Research Center, Watertown, Massachusetts 02172
2	ATTN: DRXMR-PL
1	DRXMR-PR
1	DRXMR-AP
1	DRXMR-CT
1	DRXMR-X
1	DRXMR-ER

No. of Copies	To
5	Defense Advanced Research Projects Agency, 1400 Wilson Boulevard, Arlington, Virginia 22209 ATTN: Dr. E. C. van Reuth
1	National Science Foundation, 1800 G Street, Washington, D. C. 20550 ATTN: Dr. Robert Reynik
5	General Electric Company, Corporate Research and Development, Schenectady, New York 12301 ATTN: Mr. F. X. Gigliotti, Jr.
5	Hitchiner Manufacturing Co., Inc., Elm Street, Milford, New Hampshire 03055 ATTN: Mr. G. D. Chandley
5	Abex Corporation, Research Center, Mahwah, New Jersey 07430 ATTN: H. R. Larson
5	Massachusetts Institute of Technology, Dept. of Metallurgy and Materials Science, Cambridge, Massachusetts 02139 ATTN: Dr. Merton C. Fleming
1	TRW Equipment, TRW Inc., 23555 Euclid Avenue, Cleveland, Ohio 44117 ATTN: Elizabeth Barrett, T/M 3417
1	Deposits & Composites Inc., 1821 Michael Faraday Drive, Reston, Virginia 22090 ATTN: Richard E. Engdahl, President
1	Dr. Maurice Sinnott, University of Michigan, Assoc. Dir. of Engineering, Ann Arbor, Michigan 48104
1	Fred E. Ziter, Adirondack Steel Casting Co., Shaker Road, Watervliet, New York 12189
1	Dr. Raymond J. Bratton, Westinghouse Electric Corporation Research Laboratory, Pittsburgh, Pennsylvania 15235
1	W. M. Spurgeon, Director, Mfg., Quality Control & Home Systems, Program Management Center, Bendix Research Laboratories, Bendix Center, Southfield, Michigan 48075
1	S. T. Wlodek, Director of Stellite R&D, Stellite Division, Cabot Corporation, 1020 West Park Avenue, Kokomo, Indiana 46901
1	Mr. William A. Butler, Contract Administrator, Microwave Associates, Inc., Burlington, Massachusetts 01803
1	Mr. John A. Ulrich, Sr. Vice-President, Chamberlain Manufacturing Corp., Waterloo, Iowa 50705